Figure 1 Degenerating astrocytes are located in the motor neuron microenvironment in the ventral lumbar spinal cord of hSOD1[G93A] mice. (a and b) Spheroid GFAP-positive cells (SGPCs, arrows) are located together with typical reactive astrocytes in the ventral horns of hSOD1[G93A] mice at the end stage (b), but not in the spinal cord of hSOD1[WT] transgenic mice (a); (c and d) all SGPCs are immunopositive for ubiquitin: some SGPCs exhibit continuous ubiquitin immunoreactivity in both the cell body and in the processes projecting off the cell body, which appear abnormally thick (c); cell bodies present a thick GFAP-positive cap (d); (e and f) SGPCs immunopositive for active caspase-3: notice the eccentric annular appearance of caspase-3 immunoreactivity in the cell body (e) and the thin GFAP cap (f). Scale bar, 20 μm (a and b) and 10 μm (c–f). (g) Frequency histogram shows the distribution of spheroid astrocytes around motor neurons in sections from 100-day-old mice ($n = 96$ from six mice). Distance (μm) from the closest motor neuron was measured from the border of the SGPC body to the border of the motor neuron cell body as defined by SMI32 immunostaining. Distances were put into bins of 10 μm and their frequency distribution calculated. Only 7 out of 96 SGPCs had no adjacent motor neurons, though we cannot exclude their presence in contiguous sections

positive puncta colocalized with synaptophysin ($n = 60$ fields from five mice), we concluded that, in the ventral horns of the lumbar spinal cord, VGLUT1 mostly identifies glutamatergic terminals. Using the vesicular transporter as an indicator of excitatory presynapses, we next examined the distribution of VGLUT1-positive boutons in relation to motor neurons and SGPCs. Consistent with previous reports,[20] we confirmed that

VGLUT1-immunoreactive terminals surround motor neuron cell bodies and dendrites, as defined by SMI32 staining (Figure 5b). Moreover, they enclose ubiquitin-positive SGPCs around motor cells (Figure 5c and d), suggesting that both cell types could sense glutamate released from those nerve terminals.

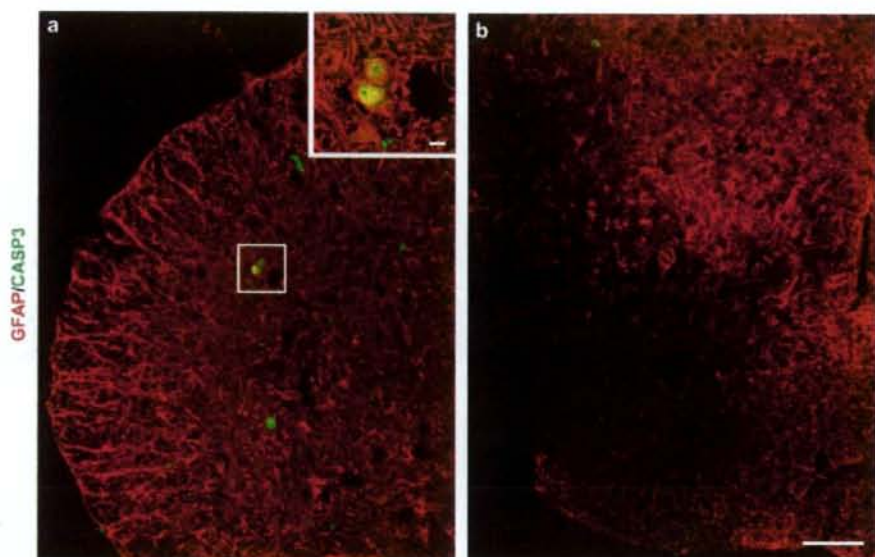Given the altered glutamate handling reported in both sporadic ALS patients and transgenic animals,[3,4,13] we

Figure 2 Degenerating astrocytes have confined distribution in the ventral region of the lumbar spinal cord. (**a** and **b**) Double immunofluorescence staining against GFAP and active caspase-3 shows the specific localization of astrocytes containing round inclusions in the ventral horns (square box magnified in inset) (**a**), but not in the dorsal horns of the lumbar spinal cord (**b**). Scale bars, 100 μm (**a** and **b**) and 10 μm (inset)
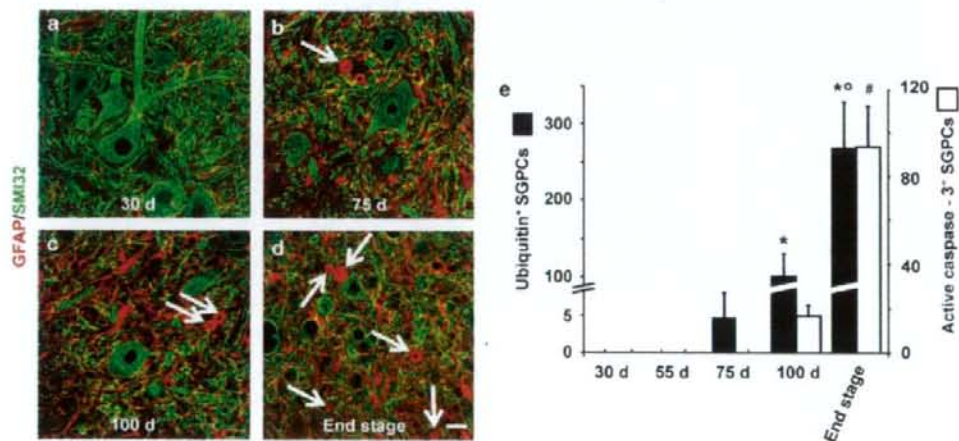

Figure 3 SGPCs appear early during disease progression in hSOD1^{G93A} mice. (**a–d**) An increasing number of SGPCs (arrows) directly contiguous to motor neurons appears during the disease progression. Lumbar spinal cord sections from mice at the age of 30 days (**a**), 75 days (**b**), 100 days (**c**) or at the end stage (**d**) were simultaneously labeled for nonphosphorylated neurofilaments (SMI32 antibody) and GFAP. Scale bar, 20 μm. (**e**) Time course of the appearance of abnormal spheroid astrocytes. Histogram represents the number of SGPCs double fluorescent for GFAP and ubiquitin (black bars) or GFAP and active caspase-3 (white bars, $n = 4$–6 mice for each time point) at different ages during the disease progression. Values are means ± S.E.M. (see Materials and Methods) (*$P < 0.05$ versus ubiquitin $^+$ SGPCs at 75 days, $^\circ P < 0.05$ versus ubiquitin $^+$ SGPCs at 100 days, $^\# P < 0.05$ versus caspase-3 $^+$ SGPCs at 100 days; ANOVA followed by the Fischer PLSD method)

investigated whether SGPCs expressed the glial glutamate transporter EAAT2/GLT1. Immunofluorescence analysis of spinal cord sections from hSOD1^{G93A} mice at the age of 100 days revealed that the SGPCs stain very weakly for this transporter (Supplementary Figure 1). Normally, expression of a highly efficient uptake system makes astrocytes resistant to glutamate concentrations toxic for neurons.[21] To verify if focal astrocytic degeneration might depend on an excitotoxic

mechanism, we prepared astrocytic cultures from the spinal cord of hSOD1^{G93A} mice and exposed them to neurotoxic glutamate concentrations (500 μM, 30 min). We found that a subpopulation of astrocytes underwent delayed caspase-3 activation and nuclear condensation. This phenomenon did not occur in sister cultures of nontransgenic or hSOD1^{WT} astrocytes (Figure 6a, left). In a different type of experiment, we transiently transfected wild-type rat spinal cord astrocytes with wild-type myc-tagged hSOD1 expression vectors (coding for hSOD1^{WT}, hSOD1^{G93A} or hSOD1^{G85R}, respectively).
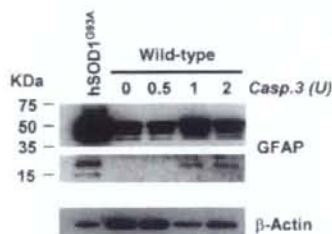

Figure 4 Active caspase-3 cleaves GFAP in the spinal cord from hSOD1^{G93A} mice but not from wild-type mice. Representative immunoblot of spinal cord homogenates from end stage hSOD1^{G93A} mice and age-matched wild-type animals. Wild-type tissues were incubated with an increasing concentration of recombinant active caspase-3 as indicated. The blot was probed with a mouse anti-GFAP monoclonal antibody that recognizes the carboxy-terminal domain of GFAP (clone G-A-5). This revealed both the full-length protein of 50 kDa and the caspase-3-cleaved GFAP fragment of 20 kDa. No labeling of the 20 kDa fragment was obtained in undigested tissue. β-actin was used as loading control

Exposure to glutamate induced delayed caspase-3 activation and nuclear condensation in both hSOD1^{G93A}- and hSOD1^{G85R}-expressing astrocytes, but not in the hSOD1^{WT}-expressing ones (Figure 6a, right). Therefore, expression of mutant hSOD1s confers glutamate vulnerability to astrocytes.

We next estimated the ambient glutamate level ([Glu]$_o$) that is toxic for mutant hSOD1-expressing astrocytes. Since in our experimental conditions cultured astrocytes express both glial glutamate transporters, EAAT1/GLAST and EAAT2/GLT1 (Supplementary Figure 2), we artificially blocked the basal glutamate uptake with the full-spectrum transport inhibitor, DL-threo-β-benzyloxyaspartate (TBOA, 200 μM, 30 min). In hSOD1^{G93A} cultures, TBOA raised [Glu]$_o$ to 1.87 $\pm$ 0.10 μM ($n = 6$ in triplicate) and triggered the death of subpopulations of astrocytes (Figure 6a, left). In wild-type astrocytes, TBOA enhanced [Glu]$_o$ to the same extent as in hSOD1^{G93A} astrocytes (to 2 $\pm$ 0.11 μM), but had no toxic effect. Therefore, ambient glutamate concentrations as low as 2 μM are selectively toxic to astrocytes expressing mutant hSOD1.

The glutamate vulnerability of mutant hSOD1-expressing astrocytes can be ascribed to mGluR5 activation. To test whether glutamate induces damage to hSOD1^{G93A} or ^{G85R}-expressing astrocytes through glutamate receptor-mediated signaling, we applied the amino acid in the presence of a mixture of glutamate receptor antagonists, the mGluR blocker (S)-α-methyl-4-carboxyphenylglycine (MCPG, 500 μM) and the AMPA/kainate receptor antagonist, 6-cyano-7-nitroquinoxaline-2,3-dione (CNQX, 10 μM; Figure 6b). This mixture completely prevented the glutamate toxicity.
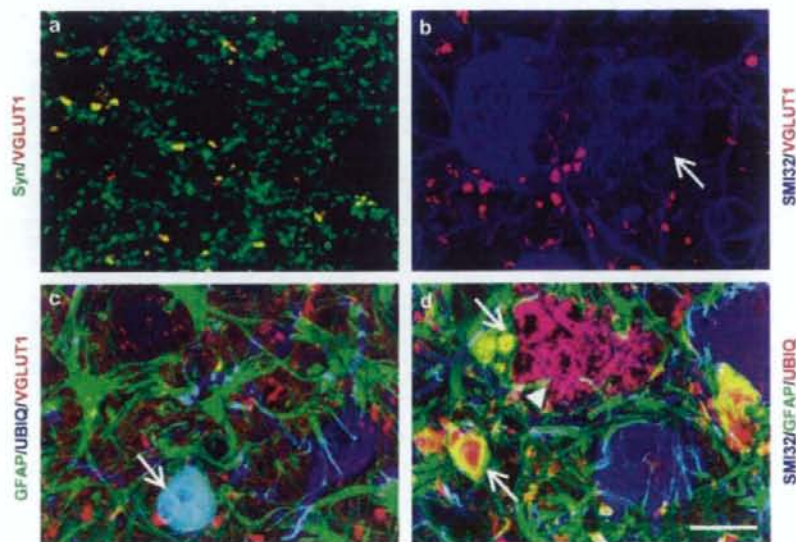

Figure 5 Degenerating astrocytes are surrounded by glutamatergic terminals immunolabeled for the vesicular glutamate transporter 1 (VGLUT1). (**a**) Representative image of spinal cord sections from hSOD1^{G93A} mice immunostained for synaptophysin (Syn) and VGLUT1. Note the massive colocalization of synaptophysin- and VGLUT1-positive puncta in the ventral horns. (**b**) Double immunostaining against SMI32 and VGLUT1 shows that VGLUT1-immunoreactive boutons end on motor neuron cell bodies and dendrites. Arrow indicates a suffering and vacuolated motor neuronal cell body. (**c** and **d**) Ubiquitin-positive SGPCs (arrows) are enclosed by glutamatergic presynaptic terminals (**c**) and they are located in the motor neuron microenvironment (**d**). Arrowhead indicates a ubiquitin-positive vacuolated motor neuron in (**d**). Scale bar, 20 μm (**a–d**)
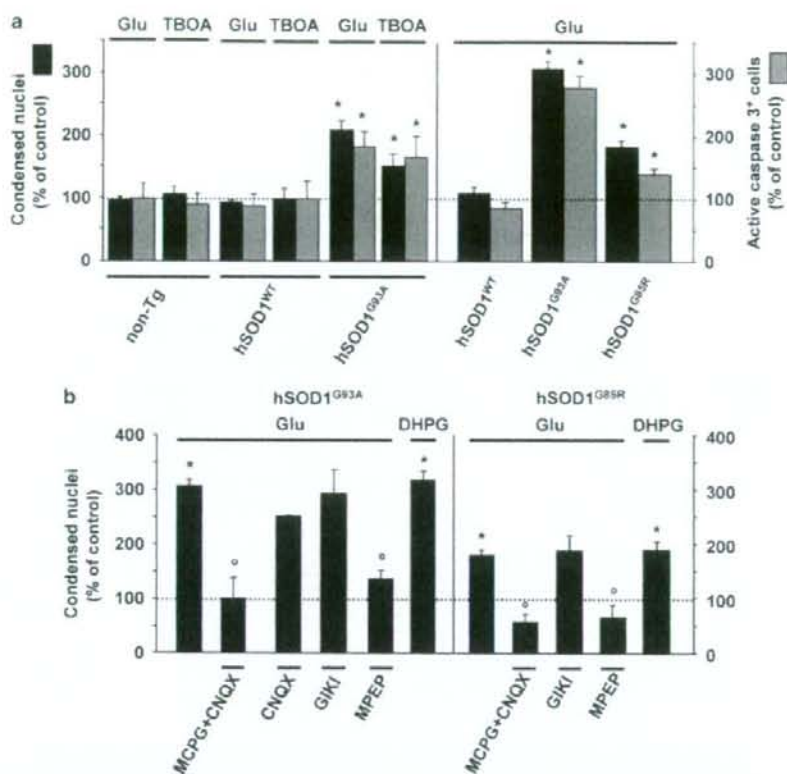
Figure 6 Expression of mutant hSOD1 confers glutamate vulnerability to spinal cord astrocytes through mGluR5-dependent signaling. (a) Left, a 30 min challenge with glutamate (500 μM) or the glutamate uptake inhibitor TBOA (200 μM) promotes within 24 h nuclear condensation (black bars) and caspase-3 activation (gray bars) in astrocyte cultures from hSOD1^{G93A} mice, but not in those from nontransgenic (non-Tg) or hSOD1^{WT} transgenic animals; (n = 3 in triplicate). Data (mean ± S.E.M.) are expressed as percentage of control, that is, the corresponding culture type challenged with saline (cells with condensed nuclei: non-Tg: 1.2 ± 0.1%; hSOD1^{WT}: 1.3 ± 0.1%; hSOD1^{G93A}: 1.2 ± 0.1%; cells immunopositive for active caspase-3: non-Tg: 0.3 ± 0.1%; hSOD1^{WT}: 0.5 ± 0.1%; hSOD1^{G93A}: 0.3 ± 0.1%, respectively). Right, transfection with cDNAs encoding hSOD1^{G93A} or hSOD1^{G85R} mutants, but not hSOD1^{WT}, confers glutamate vulnerability to normal astrocytes from the rat spinal cord. Experimental paradigm and data expression are as in the left panel (n = 7 in triplicate). Control values: cells with condensed nuclei: hSOD1^{WT}: 4.1 ± 0.4%; hSOD1^{G93A}: 3.5 ± 0.4%; hSOD1^{G85R}: 5.2 ± 0.5%; cells immunopositive for active caspase-3: hSOD1^{WT}: 6.5 ± 0.7%; hSOD1^{G93A}: 5.8 ± 0.7%; hSOD1^{G85R}: 7.4 ± 1.1%. (b) Glutamate-induced toxicity to mutant hSOD1-expressing astrocytes is selectively mediated by mGluR5 receptors. Rat spinal astrocytes transfected with either hSOD1^{G93A}-(left) or hSOD1^{G85R}-encoding (right) expression vectors were challenged with glutamate as above, in the absence (n = 7 in triplicate) or in the presence of different glutamate receptor antagonists (n = 3 per each condition), or with the group I mGluR agonist DHPG (100 μM; n = 4 in triplicate). Data are expressed as percentage of control as above (*P < 0.05 versus control (saline), °P < 0.05 versus glutamate; ANOVA followed by Fischer PLSD method)

However, individual antagonists had different effects: CNQX, as well as GYKI 52466 (50 μM), an AMPA receptor-selective blocker, did not prevent glutamate toxicity, whereas 2-methyl-6-(phenylethynyl)-pyridine (MPEP, 200 nM), a selective mGluR5 antagonist, abolished it. Accordingly, (RS)-3,5-dihydroxyphenylglycine (DHPG, 100 μM), a selective group I mGluR agonist, fully reproduced the toxic effect of glutamate (Figure 6b). Altogether, these data reveal the specific role of mGlu5 receptors in mutant hSOD1-dependent astrocyte vulnerability.

***In vivo* administration of the mGluR5 antagonist MPEP slows down astrocyte degeneration, delays disease onset and extends survival.** On the basis of the above

observations, we assessed the therapeutic efficacy of mGluR5 blockage *in vivo* in hSOD1^{G93A} transgenic mice. Starting at the age of 40 days, animals were treated daily with MPEP (30 mg/kg intraperitoneally) or saline. Thereafter, mice were monitored daily for the first signs of hindlimb muscle weakness and weekly for the decline in body weight. Weight gain stops at the time of disease onset, and is followed by a steady decrease, which strictly correlates with the decline in motor performance.[7,8] Thus, the peak in the body weight curve is taken as a measure of the earliest onset of disease.[7,8] According to this criterion, as well as to the monitoring of hindlimb muscle weakness (not shown), we found that MPEP-treated mice showed a significant delay in the onset of the disease compared with controls (saline:
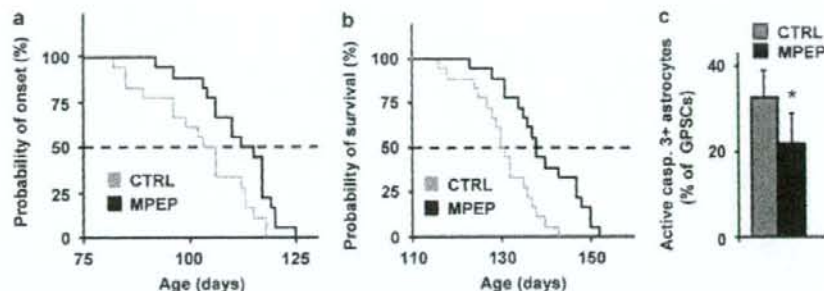
Figure 7 Treatment of hSOD1^{G93A} mice with the mGluR5 antagonist MPEP delays disease onset, extends survival and slows down astrocytic degeneration. (a and b) Kaplan–Meier curves represent the ages at which the disease onset (peak body weight) (a) and death (b) were reached for saline-treated (CTRL) and MPEP-treated (MPEP, 30 mg/kg i.p. daily) hSOD1^{G93A} mice ($n = 18$ mice for each condition). The dotted line indicates the median values in the two mouse populations. Notice that the onset of symptoms in the MPEP-treated population is significantly retarded by 9 days compared to the CTRL one ($P < 0.05$; Logrank test) and life span is extended of 7 days ($P < 0.01$; Logrank test). (c) Histograms indicate the percentage of spheroid GFAP-positive cells (SGPCs) that are active caspase-3-positive in sections from the end-stage saline-treated (CTRL) or MPEP-treated hSOD1^{G93A} mice ($n = 6$ mice for each condition). The number of caspase-3-positive cells is significantly lower in the MPEP-treated group (*$P < 0.05$; unpaired t-test)

102.4 ± 2.7 days; MPEP: 111.4 ± 2.1, days; Figure 7a). In addition, the mean survival in hSOD1^{G93A} mice treated with MPEP (138.2 ± 2.1 days) was slightly but significantly increased compared to hSOD1^{G93A} mice treated with saline (130.6 ± 1.7 days, Figure 7b). Therefore, these results prove the effectiveness of blocking the mGluR5 receptor in vivo.

To investigate whether the effects of MPEP on disease progression correlated to the focal degenerative process of astrocytes, we counted SGPCs in the ventral horns of control and MPEP-treated hSOD1^{G93A} mice at the end stage. While the total number of SGPCs was not statistically different in the two groups of animals (saline: 285 ± 34; MPEP: 258 ± 45), we found a significantly lower number of SGPCs positive for active caspase-3 in the MPEP-treated animals (saline: 93 ± 19; MPEP: 56 ± 19; Figure 7c), suggestive of a less advanced stage of astrocytic degeneration.

Discussion

An increasing body of evidence indicates that degeneration of motor neurons in ALS derives from both cell-autonomous and non-cell-autonomous processes, requiring alterations in motor neurons as well as in the surrounding nonneuronal cells, particularly microglia and astrocytes.[6] An important role for mutant hSOD1 expression in these glial cell types was recently demonstrated in hSOD1^{G37R} transgenic mice by gene excision experiments. Selective reduction of mutant hSOD1 expression in microglia slowed down the late phase of the disease.[7] Moreover, diminished expression of hSOD1 in astrocytes delayed the disease progression.[8]

The specific mechanisms by which glial cells contribute to motor neuron degeneration, however, remain elusive. Astrocytes are known to react to a variety of pathological conditions with a vigorous activation. Moreover, in ALS, they could potentially affect motor neurons in several ways, by the production of toxic species,[10,11] the concurrence to the development of excitotoxicity[12,13] and the modulation of the microglial inflammatory response.[8]

To gain further insights into the contribution of astrocytes to motor neuron degeneration, we analyzed the morphological abnormalities developed by astrocytes during ALS progression in hSOD1^{G93A} mice. By visualizing astrocytes with GFAP staining, we confirmed massive activation of astroglia throughout the spinal cord in the gray and white matter. However, we also identified a degenerative process involving a subset of astrocytes strictly confined to the microenvironment of motor neuron cell bodies, that is within the area of influence of their dendritic trees.[22] The affected cells showed unusual spheroid morphology and most of them lacked the typical GFAP-positive processes. Noteworthy, all SGPCs were strongly immunopositive for ubiquitin. This, in association with the recently described proteasome failure in the lumbar spinal cord of hSOD1^{G93A} mice,[23] may be indicative of alterations of the degradative pathways with the consequent accumulation of ubiquitinated misfolded protein inclusions within the cells. The fact that ubiquitin partially colocalizes with GFAP suggests a direct interaction between the two proteins. Thus, we deduce that GFAP is likely part of the protein aggregates, a condition which may explain the cytoskeletal disorganization identified in this subpopulation of astrocytes. At late time points, part of the SGPCs became immunopositive for active caspase-3. Importantly, a putative caspase-3 cleavage consensus DLTD^{263} site (DLTD^{266} in the human sequence) was recently identified within the GFAP amino acid sequence.[19] Cleavage in this position with generation of a 20 kDa GFAP carboxy-terminal fragment was reported in degenerating astrocytes in Alzheimer's disease.[19] Thus, we investigated whether active caspase-3 acted on the astrocytic cytoskeleton in the spinal cord of hSOD1^{G93A} transgenic mice. Using an antibody that recognizes the carboxy-terminal domain of GFAP, we could confirm that recombinant caspase-3 cleaves GFAP in vitro in nontransgenic tissues. Moreover, we detected the typical 20 kDa C-terminal fragment in the transgenic ones. Therefore, we propose that the reduced thickness of the GFAP cap and the reduced number of GFAP-positive processes in the caspase-3-positive SGPCs result from caspase-3-mediated cleavage of the astrocytic

GFAP cytoskeleton. To correlate the degenerative process identified in astrocytes with that in motor neurons, we then evaluated the time-course of appearance of SGPCs. Interestingly, we observed the first ubiquitin-positive SGPCs at 75 days of age, that is before the loss of motor cells. From that time point on, SGPC formation progressed exponentially in parallel to motor neuron degeneration. Therefore, SGPC formation has the potential to contribute to motor neuron decline and to the onset of the symptomatic phase of ALS.

Since the ventral horn gray matter presents a great abundance of excitatory afferents,[20] we decided to investigate how SGPCs interface with glutamatergic nerve terminals in the spinal cord.

In various areas of the brain, astrocytes are intimately associated with synapses, and their perisynaptic processes constitute an anatomical-functional unit, together with the presynaptic and postsynaptic elements, dubbed 'the tripartite synapse'.[24] This strategic location allows astrocytes to sense and respond to neurotransmitter spilled out of the synaptic cleft during neuronal activity.[25] Thus, glutamate released from excitatory presynapses during transmission can activate its receptors in the perisynaptic astrocytic processes and trigger neuron-glia signaling.[26,27] In addition to glial activation by synaptic spillover, there is also evidence for direct neuron-glia communication. This can occur either through the release of transmitter from presynaptic 'ectopic sites' directly facing glia,[28] or through the specific neuron-glia synaptic junctions that connect excitatory or inhibitory nerve terminals to the so-called 'NG2-glia', a peculiar type of glial cells immunopositive for the proteoglycan NG2.[29] Interestingly, studies on transgenic mice identified a group of brain cells expressing both NG2 and astrocytic markers.[30] We clearly do not know whether SGPCs derive from this population and receive direct neuronal input. This would be an attractive explanation for their selective vulnerability, but further investigations are necessary to clarify this possibility.

A number of observations indicates that glutamate handling is altered in both sporadic human ALS cases and mutant hSOD1-expressing transgenic mice, particularly due to the loss of the astrocytic glutamate transporter EAAT2/GLT1.[3,4,13]

Motor cells are potentially highly vulnerable to changes in extracellular glutamate levels as they express a large number of calcium-permeable AMPA receptors[12,31–33] and have limited capacity to buffer calcium.[34] Although astrocytes express functional glutamate receptors, they are normally more resistant to stimuli that are excitotoxic for neurons. However, in this study, we found that cultured astrocytes that express $hSOD1^{G93A}$ or $hSOD1^{G85R}$ become susceptible to concentrations of exogenous glutamate that are not detrimental for wild-type astrocytes.[21] Moreover, they degenerate in response to a moderate increase (about $2\,\mu M$) of the endogenous ambient glutamate, induced by the uptake inhibitor TBOA. Such a glutamate concentration is reached at the astrocytic membrane during the normal excitatory neurotransmission and starts glutamate receptor-mediated intracellular signaling in astrocytes.[27] Thus, it is possible that the defects of glutamate uptake in ALS – the situation mimicked by TBOA – prolong activation of astrocytic glutamate receptors and amplify the deleterious process. Noteworthy, SGPCs resulted very weakly immunopositive for EAAT2/

GLT1, suggesting a reduction of the transporter expression on these cells. A role for the metabotropic glutamate receptors in ALS was previously postulated by others.[35,36] Our data add further insight into this finding by indicating that the phenomenon herein identified, that is glutamate-dependent degeneration of mutant hSOD1-expressing astrocytes, is specifically mediated by mGluR5 in vitro. This finding is particularly interesting in view of previous observations highlighting mGluR5 abnormalities in ALS. Indeed, the expression of mGluR5 in the ventral spinal cord of ALS patients was reported to be selectively upregulated in astrocytes.[37] Moreover, astrocytes from $hSOD1^{G93A}$ rats display enhanced mGluR5 expression accompanied by alterations of the coupled signal-transduction pathways.[38] The potential relevance of our observations to ALS pathogenesis was confirmed by the studies in vivo. These showed that MPEP controls, at least in part, the degenerative process of astrocytes, reducing the number of caspase-3-positive SGPCs. In parallel, administration of MPEP delays motor decline and extends the survival of $hSOD1^{G93A}$ transgenic mice.

In conclusion, this study shows that a subpopulation of spinal astrocytes undergoes a degenerative process in ALS. This phenomenon is most likely relevant in the context of ALS pathogenesis because: (a) it is spatially restricted to astrocytes located in the microenvironment of motor neurons; (b) it starts when most motor neurons, although suffering,[39] are still alive; (c) it is sensitive to mGluR5 blockage in vivo. These observations suggest a scenario where distressed motor neurons affect the health conditions of adjacent astrocytes. Astrocytes, weakened by the expression of mutant hSOD1, become vulnerable to stimuli, such as glutamate, present in their microenvironment, and start to degenerate. This in turn may accelerate degeneration of the neighboring motor cells in an interactive process of reciprocal damage. In this context, our data complement and extend the excitotoxic hypothesis in ALS, introducing the concept that glutamatergic alterations are noxious not only to motor neurons but also to the associated astrocytes. In particular, we identify for the first time a 'gliotoxic' role of mGluR5 and a protective action of mGluR5 antagonists. This finding opens perspectives for new therapeutic approaches where mGluR5 inhibition can be combined to treatments acting on complementary mechanisms and cell targets.

Materials and Methods

Transgenic mice. Transgenic mice expressing the human $SOD1^{G93A}$ (B6SJL-TgN(SOD1-G93A)1Gur or the human $SOD1^{WT}$ (B6SJL-Tg(SOD1)2Gur/J)[2] were purchased from The Jackson Laboratories. The colonies were maintained by breeding hemizygote males to wild-type C57Bl6/SJL hybrid females (Charles River Laboratories). Offspring were genotyped and used for subsequent studies.

Histological analysis. Mice were transcardially perfused with 4% buffered paraformaldehyde and spinal cords were postfixed in the same solution. The lumbar tract was removed, paraffin embedded and sectioned at 10 μm. On selected sections, the following immunohistochemical stainings were carried out: GFAP as astrocytic marker (mouse monoclonal antibody, 1:25, Dako; rabbit polyclonal antibody, 1:1000, Dako; mouse Alexa fluor 488 conjugated monoclonal antibody, 1:1000, Chemicon), nonphosphorylated neurofilament H as neuronal marker (SMI32, mouse monoclonal antibody, 1:500, Sternberger Monoclonals Incorporated), synaptophysin (clone SY38, mouse monoclonal antibody, 1:100, Dako), VGLUT1 (rabbit polyclonal antibody, 1:3000, Synaptic Systems; rabbit polyclonal antibody fluorescence-labeled with Oyster 550, 1:1500, Synaptic

Systems), EAAT1/GLAST and EAAT2/GLT1 (rabbit polyclonal antibodies, 0.6 and 0.4 μg/ml, respectively), active caspase-3 (rabbit polyclonal antibody, 1:50, Cell Signalling), ubiquitin (rabbit polyclonal antibody, 1:300, Dako). To detect active caspase-3, a Tyramide Amplification System kit was used (NEN). For histopathological analysis, serial sections were immunostained for GFAP/ubiquitin or GFAP/active caspase-3 and positive astrocytes were counted for a total of 8–10 disectors using an unbiased stereologic physical disector technique.

Z-axis image stacks (z-step size: 0.4 μm) were collected to generate three-dimensional data sets of spinal cord sections on a Bio-Rad Radiance 2100 confocal microscope with a 60× Planapo NA1,4 oil-immersion objective in condition of optimal iris diameter as defined by LaserSharp 2000 software. To determine the spatial relationship between spheroid astrocytes and the neighboring motor neurons, image stacks were sectioned along the Z-axis using ImageJ software (National Institutes of Health) and the interdistance between the periphery of GFAP staining and the boundary of motor neuron cell body, as defined by SMI32 staining, was measured within 200 μm in spinal cord sections from 100-day-old mice. Distances were put into bins of 10 μm and their frequency of distribution were calculated.

Quantitative analysis of punctuate staining of VGLUT1 and synaptophysin was performed on images of the ventral horns of double stained sections from the mouse lumbar spinal cord. Five random 20 × 20 μm fields per each image were processed using the colocalization plugin of ImageJ software.

Caspase-3-dependent cleavage reaction. Spinal cord homogenates (10%) from end stage hSOD1[G93A] mice or age-matched wild-type littermates were prepared in PBS containing 1% CHAPS and protease inhibitors (Complete Mini, Roche). Homogenates were centrifuged at 400 × g for 10 min, supernatants were removed and stored at −80 °C.

For caspase-cleavage experiments, 20 μg of total protein were incubated for 4 h at 37 °C in cleavage buffer (50 mM Hepes pH 7.2, 50 mM NaCl, 10 mM EDTA, 0.1% CHAPS, 5% glycerol, 10 mM DTT) in the absence or in the presence of increasing concentrations of recombinant active caspase-3 (Calbiochem). Reactions were terminated by adding SDS-containing sample buffer (50 mM TrisHCl pH 6.8, 2% (w/v) SDS, 10% (v/v) glycerol, 100 mM DTT, 4% β-mercaptoethanol, 0.1% (w/v) bromophenol blue) and boiling for 10 min.

Western blot analysis. Caspase-cleaved tissues or cell lysates were electrophoresed through 10% SDS-polyacrylamide gels and transferred to nitrocellulose membranes. GFAP was detected with a mouse monoclonal antibody (clone G-A-5), which recognizes the carboxy-terminal domain of GFAP (1:500, Chemicon). EAAT1/GLAST and EAAT2/GLT1 were detected using rabbit polyclonal antibodies (0.2 and 0.1 μg/ml, respectively). β-actin was detected with a mouse monoclonal antibody (clone AC-15; 1:3000, Sigma).

Astrocyte cultures and transfection. Primary astrocyte cultures (> 99% GFAP-positive) were prepared from the spinal cord of newborn mice (hSOD1[G93A], hSOD1[WT] or nontransgenic littermates) or rats (wild-type) as described previously,[40] plated at a density of 8 × 10⁴ cells/well in 24-well plates containing glass coverslips and maintained in minimal essential medium (MEM) supplemented with 10% fetal calf serum. Confluent mouse cultures were directly used for experiments with pharmacological challenges. Rat spinal cord astrocytes were transfected 24 h after plating with the marker plasmid pEGFP-C3 (0.5 μg, Clontech Laboratories) in combination with expression vectors coding for either wild-type or mutant (G85R or G93A) c-Myc-tagged hSOD1s (1 μg). Transfection was performed with FuGENE6 Transfection Reagent (Roche). Immunocytochemical stainings using a monoclonal anti-Human c-Myc antibody (1:200, BD Biosciences Pharmingen) revealed that EGFP and c-Myc-tagged proteins colocalize in 95% of cases.

hSOD1 expression levels were determined on transfected astrocytes immunostained for c-Myc by immunofluorescence quantification as follows. Average fluorescence intensity from transfected astrocytes was measured and expressed as fluorescence intensity arbitrary units on a linear scale of 0–256 in nonsaturating condition of the camera, using the ImageJ software. Fluorescence intensity values were then expressed relative to mean fluorescence intensity obtained from the nontransfected cells (background noise).

No significant difference in the expression levels was detected between the wild-type and the mutant proteins (hSOD1[WT] expression level was set as 100%; hSOD1[G93A]: 123 ± 13.1% versus hSOD1[WT]; hSOD1[G85R]: 116.4 ± 11.8% versus hSOD1[WT]; $n = 50$ cells/genotype; values represent the mean ± S.E.M. of

three independent experiments: $P = 0.46$, one-way ANOVA). Pharmacological experiments were carried out 48 h after transfection.

Expression of the glutamate transporters EAAT1/GLAST and EAAT2/GLT1 was evaluated on astrocyte cultures fixed with 4% buffered paraformaldehyde. EAAT1/GLAST and EAAT2/GLT1 were detected using rabbit polyclonal antibodies (0.5 and 1 μg/ml, respectively). GFAP was detected with a mouse monoclonal antibody (clone G-A-5, 1:200, Chemicon).

Pharmacological treatments in vitro. Astrocyte cultures were exposed to one or combinations of the following agents for 30 min: L-Glutamate (500 μM), CNQX (10 μM), MCPG (500 μM) MPEP (200 nM), GYKI 52466 (50 μM), DHPG (100 μM), TBOA (200 μM). All agents were from Tocris Bioscience, except L-Glutamate, from Sigma. After removal of the agents, astrocytes were allowed to recover at 37 °C for 24 h.

Astrocyte toxicity assays. The toxic effect of pharmacological treatments to astrocytes in culture was determined by double staining with the fluorescent nuclear dye Hoechst 33342 (Sigma) and anti-active caspase-3 immunocytochemistry using a rabbit polyclonal antibody (Cell Signalling). The number of astrocytes showing condensed nuclei and active caspase-3 24 h after the pharmacological challenge was counted in a blind manner by two independent operators. For mouse cultures, the number of dying astrocytes was counted in 8–10 microscopic fields (40 ×) per coverslip and expressed as percentage of the total number of cells present in the field. For transfected rat astrocytes, it was expressed as percentage of the total number of transfected cells (EGFP-positive) present in the coverslip. In each experiment, 2–3 coverslips/condition were counted and experiments were replicated as indicated in the legends.

Extracellular glutamate concentration in the astrocyte cultures. Endogenous glutamate accumulated in the supernatant of astrocytes incubated with TBOA 200 μM for 30 min was measured by a specific enzymatic assay, as described previously.[40] Briefly, cell supernatant was introduced in a 1 × 1 cm cuvette (Hellma Italia) inside a LS55 computerized spectrofluorometer (Perkin-Elmer) at 37 °C under continuous stirring in a buffer containing (in mM): NaCl 120, KCl 3.1, NaH$_2$PO$_4$ 1.25, HEPES-Na 25, MgCl$_2$ 1, glucose 4, CaCl$_2$ 2 at pH 7.4, added with glutamate dehydrogenase (GDH, 15.5 U/ml) and 1 mM NADP⁺. Glutamate present in the cell medium was oxidized by GDH to α-ketoglutarate with the formation of NADPH and fluorescence emission at 430 nm (excitation light 335 nm). Glutamate was quantified referring to the standard curves constructed with exogenous glutamate.

Pharmacological treatments in vivo. hSOD1[G93A] mice were administered daily 30 mg/kg MPEP or saline intraperitoneally starting at the age of 40 days ($n = 18$ mice for each condition). Mice were thereafter kept under daily observation and weighted once a week. Since decline in peak body weight is considered the earliest observable measure of disease onset and strictly correlates with decline in motor performance,[7,8] the onset of clinical disease was defined by the achievement of peak body weight. End stage was defined as the time at which animals were unable to right themselves within 30 s when placed on their side.

1. Rosen DR, Siddique T, Patterson D, Figlewicz DA, Sapp P, Hentati A et al. Mutations in Cu/Zn superoxide dismutase gene are associated with familial amyotrophic lateral sclerosis. Nature 1993; 362: 59–62.
2. Gurney ME, Pu H, Chiu AY, Dal Canto MC, Polchow CY, Alexander DD et al. Motor neuron degeneration in mice that express a human Cu,Zn superoxide dismutase mutation. Science 1994; 264: 1772–1775.

3. Bruijn LI, Becher MW, Lee MK, Anderson KL, Jenkins NA, Copeland NG et al. ALS-linked SOD1 mutant G85R mediates damage to astrocytes and promotes rapidly progressive disease with SOD1-containing inclusions. Neuron 1997; 18: 327–338.
4. Howland DS, Liu J, She Y, Goad B, Maragakis NJ, Kim B et al. Focal loss of the glutamate transporter EAAT2 in a transgenic rat model of SOD1 mutant-mediated amyotrophic lateral sclerosis (ALS). Proc Natl Acad Sci USA 2002; 99: 1604–1609.
5. Jaarsma D, Teuling E, Haasdijk ED, De Zeeuw CI, Hoogenraad CC. Neuron-specific expression of mutant superoxide dismutase is sufficient to induce amyotrophic lateral sclerosis in transgenic mice. J Neurosci 2008; 28: 2075–2088.
6. Clement AM, Nguyen MD, Roberts EA, Garcia ML, Boillee S, Rule M et al. Wild-type nonneuronal cells extend survival of SOD1 mutant motor neurons in ALS mice. Science 2003; 302: 113–117.
7. Boillee S, Yamanaka K, Lobsiger CS, Copeland NG, Jenkins NA, Kassiotis G et al. Onset and progression in inherited ALS determined by motor neurons and microglia. Science 2006; 312: 1389–1392.
8. Yamanaka K, Chun SJ, Boillee S, Fujimori-Tonou N, Yamashita H, Gutmann DH et al. Astrocytes as determinants of disease progression in inherited amyotrophic lateral sclerosis. Nat Neurosci 2008; 11: 251–253.
9. Beers DR, Henkel JS, Xiao Q, Zhao W, Wang J, Yen AA et al. Wild-type microglia extend survival in mice with familial amyotrophic lateral sclerosis. Proc Natl Acad Sci USA 2006; 103: 16021–16026.
10. Nagai M, Re DB, Nagata T, Chalazonitis A, Jessell TM, Wichterle H et al. Astrocytes expressing ALS-linked mutated SOD1 release factors selectively toxic to motor neurons. Nat Neurosci 2007; 10: 615–622.
11. Di Giorgio FP, Carrasco MA, Siao MC, Maniatis T, Eggan K. Non-cell autonomous effect of glia on motor neurons in an embryonic stem cell-based ALS model. Nat Neurosci 2007; 10: 608–614.
12. Van Damme P, Bogaert E, Dewil M, Hersmus N, Kiraly D, Scheveneels W et al. Astrocytes regulate GluR2 expression in motor neurons and their vulnerability to excitotoxicity. Proc Natl Acad Sci USA 2007; 104: 14825–14830.
13. Rothstein JD, Van Kammen M, Levey AI, Martin LJ, Kuncl RW. Selective loss of glial glutamate transporter GLT-1 in amyotrophic lateral sclerosis. Ann Neurol 1995; 38: 73–84.
14. Guo H, Lai L, Butchbach ME, Stockinger MP, Shan X, Bishop GA et al. Increased expression of the glial glutamate transporter EAAT2 modulates excitotoxicity and delays the onset but not the outcome of ALS in mice. Hum Mol Genet 2003; 12: 2519–2532.
15. Rothstein JD, Patel S, Regan MR, Haenggeli C, Huang YH, Bergles DE et al. Beta-lactam antibiotics offer neuroprotection by increasing glutamate transporter expression. Nature 2005; 433: 73–77.
16. Pardo AC, Wong V, Benson LM, Dykes M, Tanaka K, Rothstein JD et al. Loss of the astrocyte glutamate transporter GLT1 modifies disease in SOD1(G93A) mice. Exp Neurol 2006; 201: 120–130.
17. Pasinelli P, Houseweart MK, Brown Jr RH, Cleveland DW. Caspase-1 and -3 are sequentially activated in motor neuron death in Cu,Zn superoxide dismutase-mediated familial amyotrophic lateral sclerosis. Proc Natl Acad Sci USA 2000; 97: 13901–13906.
18. Chiu AY, Zhai P, Dal Canto MC, Peters TM, Kwon YW, Prattis SM et al. Age-dependent penetrance of disease in a transgenic mouse model of familial amyotrophic lateral sclerosis. Mol Cell Neurosci 1995; 6: 349–362.
19. Mouser PE, Head E, Ha KH, Rohn TT. Caspase-mediated cleavage of glial fibrillary acidic protein within degenerating astrocytes of the Alzheimer's disease brain. Am J Pathol 2006; 168: 936–946.
20. Alvarez FJ, Villalba RM, Zerda R, Schneider SP. Vesicular glutamate transporters in the spinal cord, with special reference to sensory primary afferent synapses. J Comp Neurol 2004; 472: 257–280.
21. Choi DW, Maulucci-Gedde M, Kriegstein AR. Glutamate neurotoxicity in cortical cell culture. J Neurosci 1987; 7: 357–368.

22. Inglis FM, Furia F, Zuckerman KE, Strittmatter SM, Kalb RG. The role of nitric oxide and NMDA receptors in the development of motor neuron dendrites. J Neurosci 1998; 18: 10493–10501.
23. Kabashi E, Agar JN, Taylor DM, Minotti S, Durham HD. Focal dysfunction of the proteasome: a pathogenic factor in a mouse model of amyotrophic lateral sclerosis. J Neurochem 2004; 89: 1325–1335.
24. Araque A, Parpura V, Sanzgiri RP, Haydon PG. Tripartite synapses: glia, the unacknowledged partner. Trends Neurosci 1999; 22: 208–215.
25. Volterra A, Meldolesi J. Astrocytes: from brain glue to communication elements: the revolution continues. Nat Rev Neurosci 2005; 6: 626–640.
26. Pasti L, Volterra A, Pozzan T, Carmignoto G. Intracellular calcium oscillations in astrocytes: a highly plastic, bidirectional form of communication between neurons and astrocytes in situ. J Neurosci 1997; 17: 7817–7830.
27. Wang X, Lou N, Xu Q, Tian GF, Peng WG, Han X et al. Astrocytic Ca2+ signaling evoked by sensory stimulation in vivo. Nat Neurosci 2006; 9: 816–823.
28. Matsui K, Jahr CE. Exocytosis unbound. Curr Opin Neurobiol 2006; 16: 305–311.
29. Paukert M, Bergles DE. Synaptic communication between neurons and NG2+ cells. Curr Opin Neurobiol 2006; 16: 515–521.
30. Matthias K, Kirchhoff F, Seifert G, Huttmann K, Malyash M, Kettenmann H et al. Segregated expression of AMPA-type glutamate receptors and glutamate transporters defines distinct astrocyte populations in the mouse hippocampus. J Neurosci 2003; 23: 1750–1758.
31. Williams TL, Day NC, Ince PG, Kamboj RK, Shaw PJ. Calcium-permeable alpha-amino-3-hydroxy-5-methyl-4-isoxazole propionic acid receptors: a molecular determinant of selective vulnerability in amyotrophic lateral sclerosis. Ann Neurol 1997; 42: 200–207.
32. Van Damme P, Van Den Bosch L, Van Houtte E, Callewaert G, Robberecht W. GluR2-dependent properties of AMPA receptors determine the selective vulnerability of motor neurons to excitotoxicity. J Neurophysiol 2002; 88: 1279–1287.
33. Kawahara Y, Ito K, Sun H, Aizawa H, Kanazawa I, Kwak S. Glutamate receptors: RNA editing and death of motor neurons. Nature 2004; 427: 801.
34. Alexianu ME, Ho BK, Mohamed AH, La Bella V, Smith RG, Appel SH. The role of calcium-binding proteins in selective motoneuron vulnerability in amyotrophic lateral sclerosis. Ann Neurol 1994; 36: 846–858.
35. Anneser JM, Borasio GD, Berthele A, Zieglgansberger W, Tolle TR. Differential expression of group I metabotropic glutamate receptors in rat spinal cord somatic and autonomic motoneurons: possible implications for the pathogenesis of amyotrophic lateral sclerosis. Neurobiol Dis 1999; 6: 140–147.
36. Anneser JM, Chahli C, Borasio GD. Protective effect of metabotropic glutamate receptor inhibition on amyotrophic lateral sclerosis-cerebrospinal fluid toxicity in vitro. Neuroscience 2006; 141: 1879–1886.
37. Aronica E, Catania MV, Geurts J, Yankaya B, Troost D. Immunohistochemical localization of group I and II metabotropic glutamate receptors in control and amyotrophic lateral sclerosis human spinal cord: upregulation in reactive astrocytes. Neuroscience 2001; 105: 509–520.
38. Vermeiren C, Hemptinne I, Vanhoutte N, Tilleux S, Maloteaux JM, Hermans E. Loss of metabotropic glutamate receptor-mediated regulation of glutamate transport in chemically activated astrocytes in a rat model of amyotrophic lateral sclerosis. J Neurochem 2006; 96: 719–731.
39. Pun S, Santos AF, Saxena S, Xu L, Caroni P. Selective vulnerability and pruning of phasic motoneuron axons in motoneuron disease alleviated by CNTF. Nat Neurosci 2006; 9: 408–419.
40. Bezzi P, Domercq M, Brambilla L, Galli R, Schols D, De Clercq E et al. CXCR4-activated astrocyte glutamate release via TNFalpha: amplification by microglia triggers neurotoxicity. Nat Neurosci 2001; 4: 702–710.

Supplementary Information accompanies the paper on Cell Death and Differentiation website (http://www.nature.com/cdd)

HEPATOLOGY

Inhibition of hepatitis C virus infection and expression *in vitro* and *in vivo* by recombinant adenovirus expressing short hairpin RNA

Naoya Sakamoto,*,† Yoko Tanabe,* Takanori Yokota,‡ Kenichi Satoh,§ Yuko Sekine-Osajima,* Mina Nakagawa,*,† Yasuhiro Itsui,* Megumi Tasaka,* Yuki Sakurai,* Chen Cheng-Hsin,* Masahiko Yano,¶ Shogo Ohkoshi,¶ Yutaka Aoyagi,¶ Shinya Maekawa,†† Nobuyuki Enomoto,†† Michinori Kohara§ and Mamoru Watanabe*

Departments of *Gastroenterology and Hepatology, †Hepatitis Control, and ‡Neurology and Neurological Science, Tokyo Medical and Dental University, §Department of Microbiology and Cell Biology, The Tokyo Metropolitan Institute of Medical Science, Tokyo, ¶Gastroenterology and Hepatology Division, Graduate School of Medical and Dental Sciences, Niigata University, Niigata, and ††First Department of Medicine, Yamanashi University, Yamanashi, Japan

Abstract

Background and Aim: We have reported previously that synthetic small interfering RNA (siRNA) and DNA-based siRNA expression vectors efficiently and specifically suppress hepatitis C virus (HCV) replication *in vitro*. In this study, we investigated the effects of the siRNA targeting HCV-RNA *in vivo*.

Methods: We constructed recombinant retrovirus and adenovirus expressing short hairpin RNA (shRNA), and transfected into replicon-expressing cells *in vitro* and transgenic mice *in vivo*.

Results: Retroviral transduction of Huh7 cells to express shRNA and subsequent transfection of an HCV replicon into the cells showed that the cells had acquired resistance to HCV replication. Infection of cells expressing the HCV replicon with an adenovirus expressing shRNA resulted in efficient vector delivery and expression of shRNA, leading to suppression of the replicon in the cells by ~10^{-1}. Intravenous delivery of the adenovirus expressing shRNA into transgenic mice that can be induced to express HCV structural proteins by the Cre/*lox*P switching system resulted in specific suppression of virus protein synthesis in the liver.

Conclusion: Taken together, our results support the feasibility of utilizing gene targeting therapy based on siRNA and/or shRNA expression to counteract HCV replication, which might prove valuable in the treatment of hepatitis C.

Introduction

Hepatitis C virus (HCV), which affects 170 million people worldwide, is one of the most important pathogens causing liver-related morbidity and mortality.[1] The difficulty in eradicating HCV is attributable to limited treatment options against the virus and their unsatisfactory efficacies. Even with the most effective regimen with pegylated interferon (IFN) and ribavirin in combination, the efficacies are limited to less than half of the patients treated.[2] Given this situation, the development of safe and effective anti-HCV therapies is one of our high-priority goals.

RNA interference (RNAi) is a process of sequence-specific, post-transcriptional gene silencing that is initiated by double-stranded RNA.[3,4] Because of its potency and specificity, RNAi rapidly has become a powerful tool for basic research to analyze gene functions and for potential therapeutic applications. Recently,

successful suppression of various human pathogens by RNAi have been reported, including human immunodeficiency viruses,[5,6] poliovirus,[7] influenza virus,[8] severe acute respiratory syndrome (SARS) virus[9] and hepatitis B virus (HBV).[10–13]

We and other researchers have reported that appropriately designed small interfering RNA (siRNA) targeting HCV genomic RNA can efficiently and specifically suppress HCV replication *in vitro*.[14–19] We have tested siRNA designed to target the well-conserved 5′-untranslated region (5′-UTR) of HCV-RNA, and identified the most effective target, just upstream of the translation initiation codon. Furthermore, transfection of DNA-based vectors expressing siRNA was as effective as that of synthetic siRNA in suppressing HCV replication.[14]

In this study, we explored the further possibility that efficient delivery and expression of siRNA may be effective in suppression and elimination of HCV replication and that delivery of such
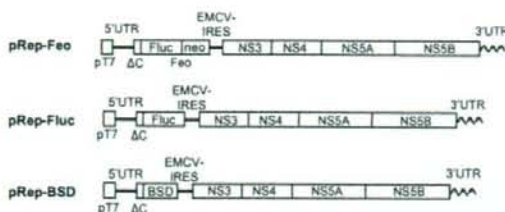
Figure 1 Structures of HCV replicon plasmids. The pRep-Feo expressed a chimeric reporter protein of firefly luciferase (Fluc) and neomycin phosphotransferase (GenBank accession No. AB119282).[14,20] The pRep-Fluc expressed the Fluc protein. The pRep-BSD expressed the blasticidin S (BSD) resistance gene. pT7, T7 promoter; 5′UTR, HCV 5′-untranslated region; ΔC, truncated HCV core region (nt. 342–377); neo, neomycin phosphotransferase gene; EMCV, encephalomyocarditis virus; NS3, NS4, NS5A and NS5B, genes that encode HCV non-structural proteins; 3′UTR, HCV 3′-untranslated region.

HCV-directed siRNA *in vivo* may be effective in silencing viral protein expression in the liver. Here, we report that HCV replication was suppressed *in vitro* by recombinant retrovirus and adenovirus vectors expressing short hairpin RNA (shRNA) and that the delivery of the adenovirus vector to mice *in vivo* specifically inhibited viral protein synthesis in the liver.

Methods

Cells and cell culture

Huh7 and Retro Pack PT67 cells (Clontech, Palo Alto, CA, USA) were maintained in Dulbecco's modified minimal essential medium (Sigma, St. Louis, MO, USA) supplemented with 10% fetal calf serum at 37°C under 5% CO_2. To maintain cell lines carrying the HCV replicon, G418 (Wako, Osaka, Japan) was added to the culture medium to a final concentration of 500 μg/mL.

HCV replicon constructs and transfection

HCV replicon plasmids, pRep-Feo, pRep-Fluc and pRep-BSD were constructed from were constructed from a virus, HCV-N strain, genotype 1b.[21] The pRep-Feo expressed a chimeric reporter protein of firefly luciferase (Fluc) and neomycin phosphotransferase.[14,20] The pRep-Fluc and the pRep-BSD expressed the Fluc and blasticidin S (BSD) resistance genes, respectively (Fig. 1). The replicon RNA synthesis and the transfection protocol have been described previously.[22]

Synthetic siRNA and siRNA-expression plasmid

The design and construction of HCV-directed siRNA vectors have been described.[14] Briefly, five siRNA targeting the 5′-UTR of HCV RNA were tested for their efficiency to inhibit HCV replication, and the most effective sequence, which targeted nucleotide position of 331 though 351, was used in the present study. To construct shRNA-expressing DNA cassettes, oligonucleotide inserts were synthesized that contained the loop sequence (5′-TTC AAG AGA-

3′) flanked by sense and antisense siRNA sequences (Fig. 2a). These were inserted immediately downstream of the human U6 promoter. To avoid a problem in transcribing shRNA because of instability of the DNA strands arising from the tight palindrome structure, several C-to-T point mutations, which retained completely the silencing activity of the shRNA, were introduced into the sense strand of the shRNA sequences (referred to as 'm').[23] A control plasmid, pUC19-shRNA-Control, expressed shRNA directed towards the Machado–Joseph disease gene, which is a mutant of ataxin-3 gene and is not normally expressed. We have previously described the sequence specific activity of the shRNA-Control.[24]

Prior to construction of the virus vectors, we tested silencing efficiency of five shRNA constructs of different lengths that covered the target sequence (Fig. 2a). The shRNA-HCV-19, shRNA-HCV-21 and shRNA-HCV-27 had target sequences of 19, 21 and 27 nucleotides, respectively. Transfection of these shRNA constructs into Huh7/pRep-Feo showed that shRNA with longer target sequences had better suppressive effects (Fig. 2b). Therefore, we used shRNA-HCV-27m (abbreviated as shRNA-HCV) in the following study.

Recombinant retrovirus vectors

The U6-shRNA expression cassettes were inserted into the *Stu*I/*Hind*III site of a retrovirus vector, pLNCX2 (Clontech) to construct pLNCshRNA-HCV and pLNCshRNA-Control (Fig. 2c). The plasmids were transfected into the packaging cells, Retro Pack PT67. The culture supernatant was filtered and added onto Huh7 cells with 4 μg/mL of polybrene. Huh7 cell lines stably expressing shRNA were established by culture in the presence of 500 μg/mL of G418.

Recombinant adenovirus

Recombinant adenoviruses expressing shRNA were constructed using an Adenovirus Expression Vector Kit (Takara, Otsu, Japan). The U6-shRNA expression DNA cassette was inserted into the *Swa*I site of pAxcw to construct pAxshRNA-HCV and pAxshRNA-Control. The adenoviruses were propagated according to the manufacturer's protocol (AxshRNA-HCV and AxshRNA-Control; Fig. 2c). A 'multiplicity of infection' (MOI) was used to standardize infecting doses of adenovirus. The MOI stands for the ratio of infectious virus particles to the number of cells being infected. An MOI = 1 represents equivalent dose to introduce one infectious virus particle to every host cell that is present in the culture.

Plasmids for assays of interferon responses

pISRE-TA-Luc (Invitrogen, Carlsbad, CA, USA) contained five copies of the consensus interferon stimulated response element (ISRE) motifs upstream of the Fluc gene. pTA-Luc (Invitrogen), which lacks the enhancer element, was used for background determination. The pcDNA3.1 (Invitrogen) was used as an empty vector for mock transfection. pRL-CMV (Promega, Madison, WI, USA), which expresses the *Renilla* luciferase protein, was used for normalization of transfection efficiency.[25] A plasmid, peGFPneo (Invitrogen), was used to monitor percentages of transduced cells.
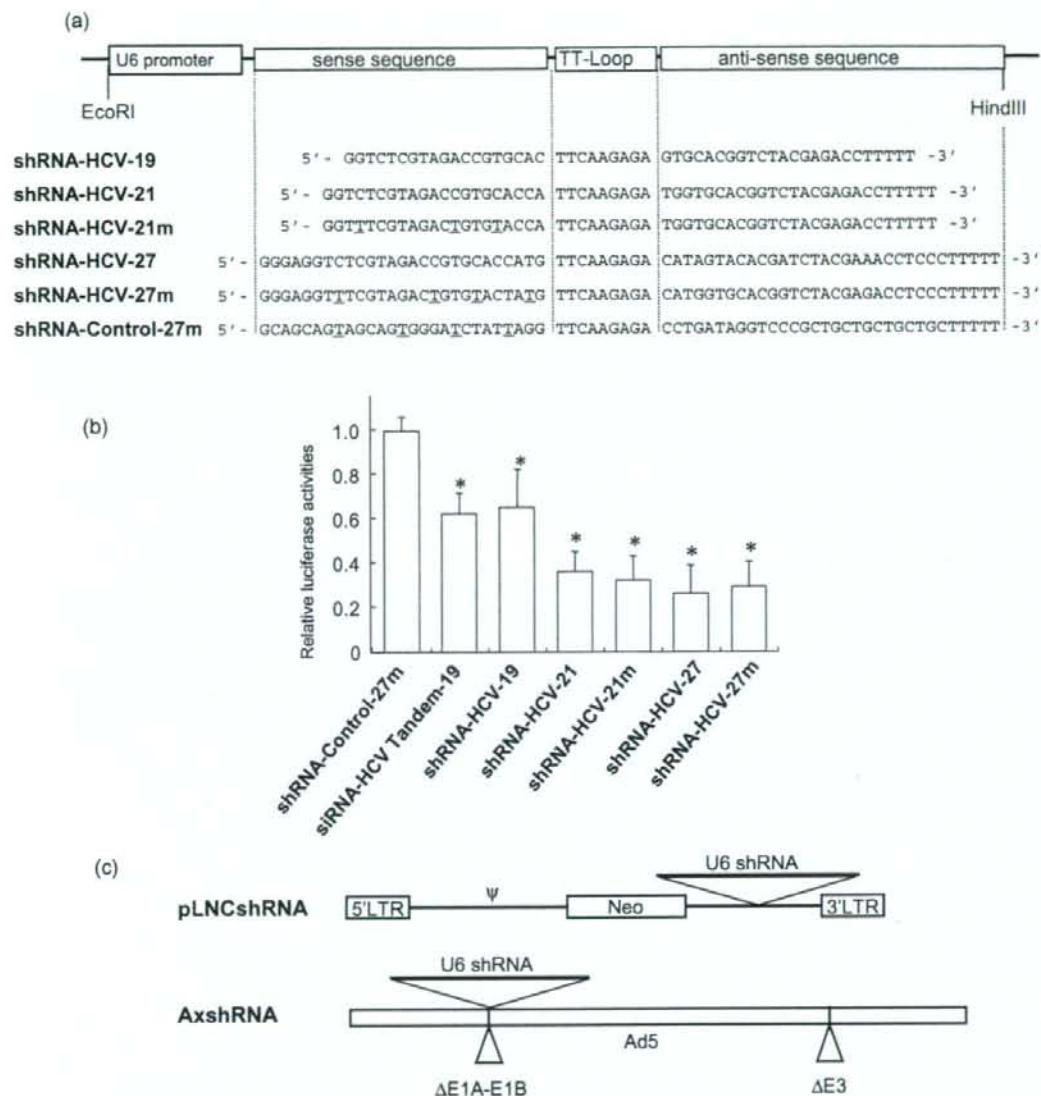
Figure 2 Structure of shRNA-expression constructs and shRNA sequences. (a) Structure of shRNA-expression cassette and shRNA sequences. TT-Loop, the loop sequence. The shRNA-Control was directed toward an unrelated target, Machado–Joseph disease gene. Underlined letters indicate C-to-T point mutations in the sense strand. (b) The shRNA-expression plasmids were transfected into Huh7/pRep-Feo cells, and internal luciferase activities were measured at 48 h of transfection. Each assay was done in triplicate, and the values are displayed as mean + SD. $*P < 0.05$. (c) pLNCshRNA, structure of a recombinant retrovirus expressing shRNA. Ψ, the retroviral packaging signal sequence. AxshRNA, structure of a recombinant adenovirus expressing shRNA.

Real-time RT-PCR analysis

Total cellular RNA was extracted from cultured cells or liver tissue using ISOGEN (Nippon Gene, Tokyo, Japan). Total cellular RNA (2 µg) was used to generate cDNA from each sample using the SuperScript II reverse-transcriptase (Invitrogen). The mRNA expression levels were measured using the Light Cycler PCR and detection system (Roche, Mannheim, Germany) and Light Cycler Fast Start DNA Master SYBR Green 1 mix (Roche).

Luciferase assays

Luciferase activity was measured using a luminometer, Lumat LB9501 (Promega) and the Bright-Glo Luciferase Assay System (Promega) or the Dual-Luciferase Reporter Assay System (Promega).

Northern and western hybridization

Total cellular RNA was separated by denaturing agarose-formaldehyde gel electrophoresis, and transferred to a nylon membrane. The membrane was hybridized with a digoxigenin-labeled probe specific for the full-length replicon sequence, and subsequently with a probe specific for beta-actin. The signals were detected by chemiluminescence reaction using a Digoxigenin Luminescent Detection Kit (Roche), and visualized by Fluoro-Imager (Roche). For the western blotting, 10 µg of total cell lysate was separated on NuPAGE 4.12% Bis-TrisGel (Invitrogen), and blotted onto an Immobilon PVDF Membrane (Roche). The membrane was incubated with monoclonal antibodies specific for HCV-NS5A (BioDesign, Saco, ME, USA), NS4A (Virogen, Watertown, MA, USA), or beta-actin (Sigma), and detected by a chemiluminescence reaction (BM Chemiluminescence Blotting Substrate; POD, Roche).

Transient-replication assays

A replicon, pRep-Fluc, was transfected into cells and the luciferase activities of the cell lysates were measured serially. To correct the transfection efficiency, each value was divided by the luciferase activity at 4 h after the transfection.

Stable colony formation assays

Cells were transfected with a replicon, pRep-BSD, and were cultured in the presence of 150 µg/mL of BSD (Invitrogen). BSD-resistant cell colonies appeared after ~3 weeks of culture, and were counted.

HCV-JFH1 virus cell culture

An *in-vitro* transcribed HCV-JFH1 RNA[26] was transfected into Huh7.5.1 cells.[27] Naive Huh7.5.1 cells were subsequently infected by the culture supernatant of the JFH1-RNA transfected Huh-7.5.1 cells, and subjected to siRNA or drug treatments. Replication levels of HCV-RNA were quantified by the realtime RT-PCR by using primers that targeted HCV-NS5B region, HCV-JFH1 sense: 5′-TCA GAC AGA GCC TGA GTC CA-3′, and HCV-JFH1 antisense: 5′-AGT TGC TGG AGG GCT TCT GA-3′.

Mice and adenovirus infection

Transgenic mice, CN2-29, inducibly express mRNA for the HCV structural proteins (genotype1b, nucleotides 294–3435) by the Cre/loxP switching system.[28] The transgene does not contain full-length HCV 5′-UTR, but shares the target sequence of the shRNA-HCV. Although the transgenic mouse CN2 has been previously reported as expressing higher levels of the viral proteins, the expression levels of the viral core protein in the CN2-29 mice are modest and similar to that in the liver of HCV patients. Thus, we chose CN2-29 mice in the present study.

The mice were infected with AxshRNA-HCV or controls (AxshRNA-Control or AxCAw1) in combination with AxCAN-Cre, which expressed Cre recombinase. Three days after the infection, the mice were killed and HCV core protein in the liver was measured as described below. The BALB/c mice were maintained in the Animal Care Facility of Tokyo Medial and Dental University, and transgenic mice were in the Tokyo Metropolitan Institute of Medical Science. Animal care was in accordance with institutional guidelines. The review board of the university approved our experimental animal studies and all experiments were approved by the institutional animal study committees.

Measurement of HCV core protein in mouse liver

The amounts of HCV core protein in the liver tissue from the mice was measured by a fluorescence enzyme immunoassay (FEIA)[29] with a slight modification. Briefly, the 5F11 monoclonal anti-HCV-core antibody was used as the first antibody on the solid phase, and the 5E3 antibody conjugated with horseradish peroxidase was the second antibody. This FEIA can detect as little as 4 pg/mL of recombinant HCV-core protein. Contents of the HCV core protein in the liver samples were normalized by the total protein contents and expressed as pg/mg total protein.

Immunohistochemical staining

Liver tissue was frozen with optimal cutting temperature (OTC) compound (Tissue Tek; Sakura Finetechnical, Tokyo, Japan). The sections (8 µm thick) were fixed with a 1:1 solution of acetone : methanol at −20°C for 10 min and then washed with phosphate-buffered saline (PBS). Subsequently, the sections were incubated with the IgG fraction of an anti-HCV core rabbit polyclonal antibody (RR8)[28] in blocking buffer or antialbumin rabbit polyclonal antibody (Dako Cytomation, Glostrup, Denmark) in PBS overnight at 4°C. The sections were incubated with secondary antibody, Alexa-antirabbit IgG (Invitrogen) or TRITIC-antirabbit IgG (Sigma), for 2 h at room temperature. Fluorescence was observed using a fluorescence microscope.

Statistical analyses

Statistical analyses were performed using Student's *t*-test; *P*-values of less than 0.05 were considered to be statistically significant.

Results

Retrovirus transduction of shRNA can protect from HCV replication

Retrovirus vectors propagated from pLNCshRNA-HCV and pLNCshRNA-Control were used to infect Huh7 cells, and cell lines were established that constitutively express shRNA-HCV and shRNA-Control (Huh7/shRNA-HCV and Huh7/shRNA-Control, respectively). There were no differences in the cell morphology or growth rate between shRNA-transduced and non-transduced Huh7 cells (data not shown). The HCV replicon, pRep-Fluc, was transfected into Huh7/shRNA-HCV, Huh7/shRNA-Control and naive Huh7 cells by electroporation. In Huh7/shRNA-Control and naive Huh7 cells, the initial luciferase activity at 4 h decreased temporarily, which represents decay of the transfected replicon RNA, but increased again at 48 h and 72 h, which demonstrate de novo synthesis of the HCV replicon RNA. In contrast, transfection into Huh7/shRNA-HCV cells resulted in a decrease in the initial luciferase activity, reaching background by 72 h (Fig. 3a). Similarly, transfection of the replicon, pRep-BSD, into Huh7 cells and BSD selection yielded numerous BSD-resistant colonies in the naive Huh7 (832 colonies) and Huh7/shRNA-Control cell lines (740 colonies), while transfection of Huh7/shRNA-HCV, which expressed shRNA-HCV, yielded obviously fewer colonies (five colonies), indicating reduction of colony forming units by ~10^2 (Fig. 3b). There was no difference in shape, growth or viability between cells expressing the shRNA or not. These results indicated that cells expressing HCV-directed shRNA following retrovirus transduction acquired resistance to HCV replication.

Effect of recombinant adenoviruses expressing shRNA on *in vitro* HCV replication

We investigated subsequently the effects of recombinant adenovirus vectors expressing shRNA. AxshRNA-HCV and AxshRNA-Control were used separately to infect Huh7/pRep-Feo cells, and the internal luciferase activities were measured sequentially (Fig. 4a). AxshRNA-HCV caused continuous suppression of HCV RNA replication. Six days postinfection, the luciferase activities fell to background levels. In contrast, the luciferase activities of the Huh7/pRep-Feo cells infected with AxshRNA-Control did not show any significant changes compared with untreated Huh7/pRep-Feo cells (Fig. 4a). The dimethylthiazol carboxymethoxyphenyl sulfophenyl tetrazolium (MTS) assay showed no significant difference between cells that were infected by recombinant adenovirus and uninfected cells (Fig. 4b). In the northern blotting analysis, the cells were harvested 6 days after infection with the adenovirus at an MOI of 1. Feo-replicon RNA of 9.6 kb, which was detectable in the untreated Huh7/pRep-Feo cells and in the cells infected with AxshRNA-Control, diminished substantially following infection with the AxshRNA-HCV (Fig. 4c). Densitometries showed that the intracellular levels of the replicon RNA in the Huh7/pRep-Feo cells correlated well with the internal luciferase activities. Similarly in the western blotting, cells were harvested 6 days after infection with adenovirus. Levels of the HCV NS4A and NS5A proteins that were translated from the HCV replicon decreased following infection with the AxshRNA-HCV
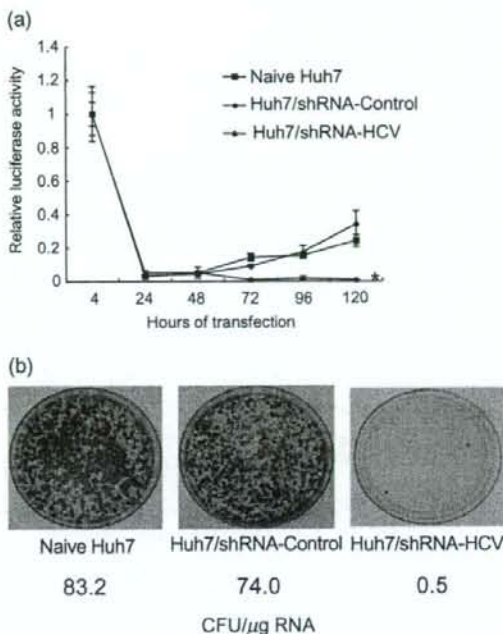
(a)

(b)

Naive Huh7	Huh7/shRNA-Control	Huh7/shRNA-HCV
83.2	74.0	0.5

CFU/µg RNA

Figure 3 HCV replication can be inhibited by shRNA-HCV which was stably transfected into cells. Huh7/shRNA-HCV and Huh7/shRNA-Control stably express shRNA-HCV or shRNA-Control, respectively, following retroviral transduction. (a) Transient replication assay. An HCV replicon RNA, pRep-Fluc, was transfected into naive Huh7, Huh7/shRNA-HCV and Huh7/shRNA-Control cells. Luciferase activities of the cell lysates were measured serially at the times indicated, and the values were plotted as ratios relative to luciferase activities at 4 h. The luciferase activities at 4 h represent transfected replicon RNA. The data are mean ± SD. An asterisk denotes a *P*-value of less than 0.001 compared with the corresponding value of the naive Huh7 cells. (b) Stable colony formation assay. The HCV replicon, pRep-BSD, was transfected into naive Huh7, Huh7/shRNA-HCV and Huh7/shRNA-Control cells. The cells were cultured in the presence of blasticidin S (BSD) in the medium for ~3 weeks, and the BSD-resistant colonies were counted. These assays were repeated twice. The colony-forming units per microgram RNA (CFU/µg RNA) are shown at the bottom.

(Fig. 4d). These results indicated that the decrease in luciferase activities was due to specific suppressive effects of shRNA on expression of HCV genomic RNA and the viral proteins, and not due to non-specific effects caused by the delivery of shRNA or to toxicity of the adenovirus vectors.

Absence of interferon-stimulated gene responses by siRNA delivery

It has been reported that double-stranded RNA may induce interferon-stimulated gene (ISG) responses which cause instability of mRNA, translational suppression of proteins and apoptotic cell

(a)

(b)

(c)

(d)
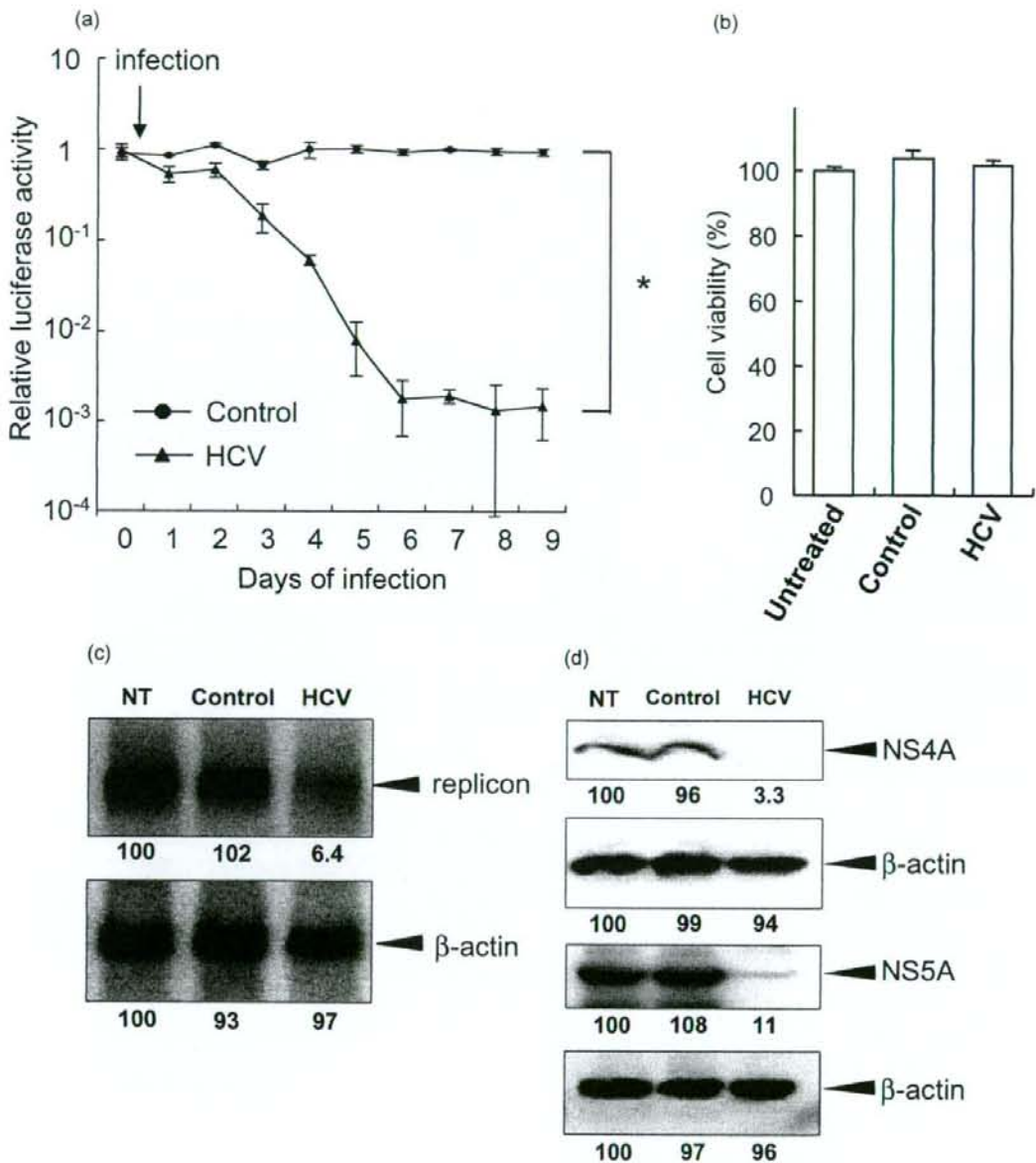
death.[18,30,31] Therefore, we examined the effects of the shRNA-expressing plasmids and adenoviruses on the activation of ISG expression in cells. The ISRE-reporter plasmid, pISRE-TA-Luc, and a control plasmid, peGFPneo, were transfected into Huh7 cells with plasmid pUC19-shRNA-HCV or pUC19-shRNA-Control, or adenovirus, AxshRNA-HCV or AxshRNA-Control, and the ISRE-mediated luciferase activities were measured. On day 2, the ISRE-luciferase activities did not significantly change in cells in which

Figure 4 Effect of a recombinant adenovirus expressing shRNA on HCV replicon. (a) Huh7/pRep-Feo cells were infected with AxshRNA-HCV or shRNA-Control at a multiplicity of infection (MOI) of 1. The cells were harvested, and internal luciferase activities were measured on day 0 though day 9 after adenovirus infection. Each assay was done in triplicate, and the value is displayed as a percentage of no treatment and as mean ± SD. An asterisk indicates a *P*-value of less than 0.05. (b) Dimethylthiazol carboxymethoxyphenyl sulfophenyl tetrazolium (MTS) assay of Huh7/pRep-Feo cells. Cells were infected with indicated recombinant adenoviruses at an MOI of 1. The assay was done at day 6 of infection. Error bars indicate mean + SD. (c) Northern blotting. The upper panel shows replicon RNA, and the lower panel shows beta-actin mRNA. (d) Western blotting. Total cell lysates were separated on NuPAGE gel, blotted and incubated with monoclonal anti-NS4A or anti-NS5A antibodies. The membrane was re-blotted with antibeta-actin antibodies. NT, untreated Huh7/pRep-Feo cells; Control, cells infected with AxshRNA-Control; HCV, cells treated with AxshRNA-HCV. In panels (b) and (c), cells were harvested on day 6 after adenovirus infection at an MOI of 1.
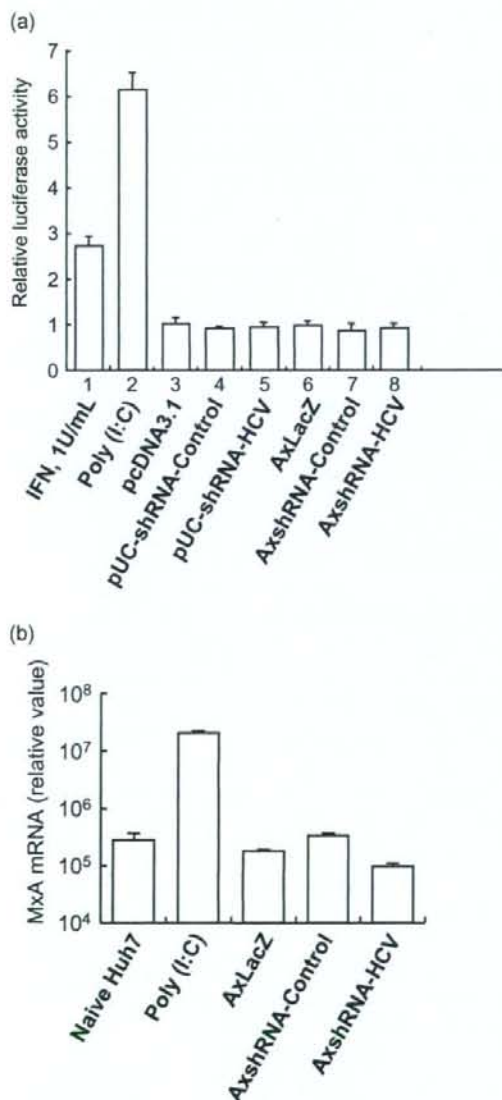
(a)

Figure 5 Interferon-stimulated gene responses by transfection of siRNA vectors. (a) Huh7 cells were seeded at 5×10^4 per well in 24-well plates on the day before transfection. As a positive control, 200 ng of pISRE-TA-Luc, or pTA-Luc, 1 ng of pRL-CMV, were transfected into a well using FuGENE-6 Transfection Reagent (Roche), and the cells were cultured with 1 U/mL of interferon (IFN) in the medium (lane 1). Lanes 3–5: 200 ng of pISRE-TA-Luc or pTA-Luc, and 1 ng of pRL-CMV were cotransfected with (lane2) 300 ng of poly (I : C), or 200 ng of plasmids (lane 3) pcDNA3.1, (lane 4) pUC19-shRNA-Control or (lane 5) pUC19-shRNA-HCV. Lanes 6–8: 200 ng of pISRE-TA-Luc or pTA-Luc, and 1 ng of pRL-CMV were transfected, and MOI = 1 of adenoviruses, (lane 6) AxLacZ, which expressed the beta-galactosidase (LacZ) gene under control of the chicken beta-actin (CAG) promoter as a control, (lane 7) AxshRNA-Control or (lane 8) AxshRNA-HCV were infected. Dual luciferase assays were performed at 48 h after transfection. The Fluc activity of each sample was normalized by the respective Rluc activity, and the respective pTA luciferase activity was subtracted from the pISRE luciferase activity. The experiment was done in triplicate, and the data are displayed as means + SD. (b) Huh7 cells were infected with indicated recombinant adenoviruses, AxLacZ, AxshRNA-Control and AxshRNA-HCV. RNA was extracted from each sample at day 6, and mRNA expression levels of an interferon-inducible MxA protein were quantified by the real-time RT-PCR analysis. Primers used were as follows: human MxA sense, 5′-CGA GGG AGA CAG GAC CAT CG-3′; human MxA antisense, 5′-TCT ATC AGG AAG AAC ATT TT-3′; human beta-actin sense, 5′-ACA ATG AAG ATC AAG ATC ATT GCT CCT CCT-3′; and human beta-actin antisense, 5′-TTT GCG GTG GAC GAT GGA GGG GCC GGA CTC-3′.

(b)

negative- or positive-control shRNA plasmids was transfected. (Fig. 5a). Similarly, the expression levels of an interferon-inducible MxA protein did not significantly change by transfection of shRNA-expression vectors (Fig. 5b). These results demonstrate that the shRNA used in the present study lack induction of the ISG responses both in the form of the expression plasmids and the adenovirus vectors.

Effect of siRNA and shRNA adenoviruses on HCV-JFH1 cell culture

The effects of HCV-targeted siRNA- and shRNA-expressing adenoviruses were confirmed by using HCV-JFH1 virus cell culture system. Transfection of the siRNA #331[14] into HCV-infected Huh7.5.1 cells resulted in substantial decrease of intracellular HCV RNA, while a control siRNA showed no effect (Fig. 6a). Similarly, infection of AxshRNA-HCV into Huh7.5.1/HCV-JFH1 cells specifically suppressed expression of HCV RNA (Fig. 6b).
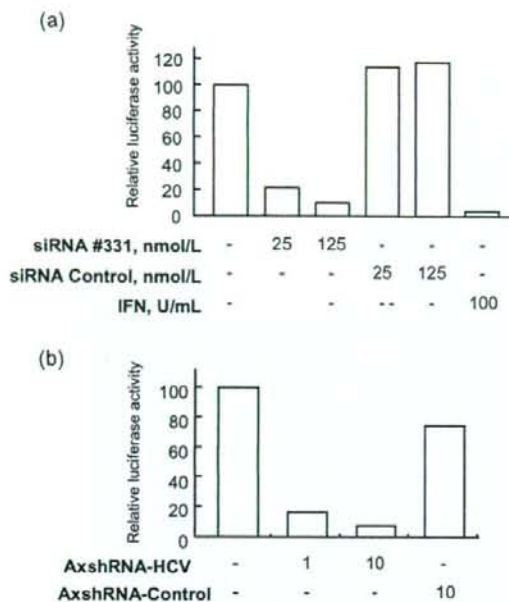
(a)

siRNA #331, nmol/L	-	25	125	-	-	-
siRNA Control, nmol/L	-	-	-	25	125	-
IFN, U/mL	-	-	-	--	-	100

(b)

AxshRNA-HCV	-	1	10	-
AxshRNA-Control	-	-	-	10

Figure 6 Effects of an siRNA and adenovirus expressing shRNA on HCV-JFH1 cell culture. (a) The siRNA #331, the siRNA-Control[14], (b) AxshRNA-HCV or AxshRNA-Control were, respectively, transfected or infected onto HV-JFH1-infected Huh7.5.1 cells. Seventy-two hours of the transfection or infection, expression level of HCV-RNA was quantified by real-time RT-PCR. The assays were repeated twice, and consistent results were obtained. IFN, recombinant interferon-alpha 2b.

Suppression of HCV-IRES-mediated translation *in vivo* by adenovirus expressing shRNA

The effects of the shRNA expression on the expression of the viral structural proteins *in vivo* were investigated using conditional HCV cDNA-transgenic mice, CN2-29.[28] Adenoviruses, AxshRNA-HCV, AxshRNA-Control or AxCAw1 were injected into CN2-29 mice in combination with AxCANCre, an adenovirus expressing *Cre* DNA recombinase. The mice were killed on the fourth day after the injection, and the hepatic expression of the HCV core protein was measured. The expressed amounts of the core protein were 143.0 ± 56.2 pg/mg and 108.5 ± 42.4 pg/mg in AxCAw1 and AxshRNA-Control-infected mice, respectively, and the expressed amount was significantly lower in mice injected with AxshRNA-HCV (28.7 ± 7.0 pg/mg, $P < 0.05$, Fig. 7a). Similarly, the induced expression of HCV core protein was not detectable by immunohistochemistry in AxshRNA-HCV infected liver tissue (Fig. 7c). Staining of a host cellular protein, albumin, was not obviously different between the liver infected with AxCAw1, AxshRNA-HCV and AxshRNA-Control (Fig. 7d). The expression levels of two ISG, IFN-beta and Mx1, in the liver tissue were not significantly different between individuals with

and without injection of the adenovirus vectors (Fig. 7b). These results indicate specific shRNA silencing of HCV structural protein expression in the liver.

Discussion

The requirements to achieve a high efficiency using RNAi are: (i) selection of target sequences that are the most susceptible to RNAi; (ii) persistence of siRNA activity; and (iii) efficient *in vivo* delivery of siRNA to cells. We have used an shRNA sequence that was derived from a highly efficient siRNA (siRNA331), and constructed a DNA-based shRNA expression cassette that showed competitive effects with the synthetic siRNA (Fig. 2).[14] The shRNA-expression cassette does not only allow extended half-life of the RNAi, but also enables use of gene-delivery vectors, such as virus vectors. As shown in the results, a retrovirus vector expressing shRNA-HCV could stably transduce cells to express HCV-directed shRNA, and the cells acquired protection against HCV subgenomic replication (Fig. 3). An adenovirus vector expressing shRNA-HCV resulted in suppression of HCV subgenomic and protein expression by around three logs to almost background levels (Fig. 4). Consistent results were obtained by using an HCV cell culture (Fig. 6). More importantly, we have demonstrated *in-vivo* effects on viral protein expression in the liver using a conditional transgenic mouse model (Fig. 7). These results suggest that efficient delivery of siRNA could be effective against HCV infection *in vivo*.

An obstacle to applying siRNA technology to treat virus infections is that viruses are prone to mutate during their replication.[32] HCV continuously produces mutated viral strains to escape immune defense mechanisms. Even in a single patient, the circulating HCV population comprises a large number of closely related HCV sequence variants called quasispecies. Therefore, siRNA targeting the protein-coding sequence of the HCV genome, which have been reported by others,[15–19] may vary considerably among different HCV genotypes, and even among strains of the same genotype.[33] Our shRNA sequence targeted the 5′-UTR of HCV RNA, which is the most conserved region among various HCV isolates.[33] In addition, the structural constraints on the 5′-UTR, in terms of its requirement to direct internal ribosome entry and translation of viral proteins, might not permit the evolution of escape mutations. Our preliminary results have shown that the siRNA-HCV suppressed replication of an HCV genotype 2a replicon[34] to the same extent as the HCV 1b replicon.

Although the siRNA techniques rely on a high degree of specificity, several studies report siRNA-induced non-specific effect that may result from induction of ISG responses.[18,31] These effects may be mediated by activation of double-strand RNA-dependent protein kinase, toll-like receptor 3,[35] or possibly by a recently identified RNA helicase, RIG-I.[36] It remains to be determined whether these effects are generally induced by every siRNA construct. Sledz *et al.* have reported that transfection of two siRNA induced cellular interferon responses,[37] while Bridge *et al.* report that shRNA-expressing plasmids induced an interferon response but transfection of synthetic siRNA did not.[31] Speculatively, these effects on the interferon system might be construct dependent. Our shRNA-expression plasmids and adenoviruses did not activate ISG responses *in vitro* (Fig. 5a,b) or *in vivo* (Fig. 7b). We have preliminarily detected phosphorylated PKR (P-PKR) by western
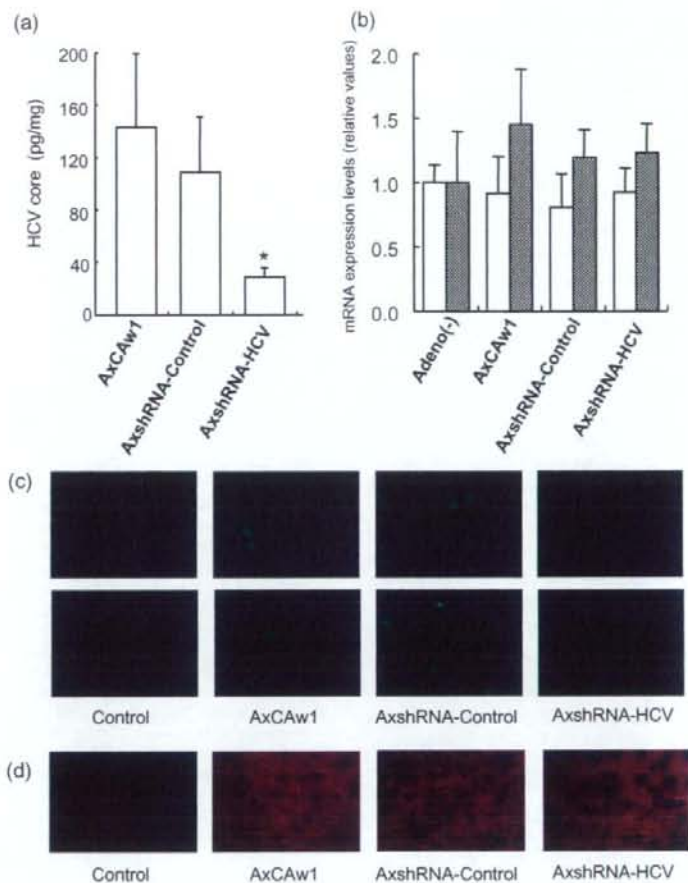
Figure 7 Effects of a recombinant adenovirus expressing shRNA on HCV core protein expression in CN2-29 transgenic mice. CN2-29 transgenic mice were administered with 1×10^9 PFU of AxCANCre combined with 6.7×10^8 PFU of AxshRNA-HCV, AxshRNA or AxCAw1. The mice were killed on day 4 after injection. (a) Quantification of HCV core protein in liver. Liver tissues were homogenized and used to determine the amount of HCV core protein. Each assay was done in triplicate, and the values are displayed as mean ± SD. Asterisk indicates *P*-value of less than 0.05. (b) Expression levels of mouse interferon-beta (white bars) and Mx1 (shaded bars) mRNA in the mouse liver tissue were quantified by the real-time RT-PCR analyses. Primers used were as follows: mouse interferon-beta sense, 5′-ACA GCC CTC TCC ATC AAC TA-3′; mouse interferon-beta antisense, 5′-CCC TCC AGT AAT AGC TCT TC-3′; mouse Mx1 sense, 5′-AGG AGT GGA GAG GCA AAG TC-3′; mouse Mx1 antisense, 5′-CAC ATT GCT GGG GAC TAC CA-3′; mouse beta-actin sense, 5′-ACT CCT ATG TGG GTG ACG AG-3′; mouse beta-actin antisense, 5′-ATA GCC CTC GTA GAT GGG CA-3′. Adeno (-) denotes mice without adenovirus administration. (c) Immunofluorescence microscopy of HCV core protein in the liver tissue. Liver sections of mice were stained using rabbit anticore polyclonal antibody and normal rabbit IgG as a negative control. The upper photographs were obtained at 400× magnification, and the lower photographs were at 1000×. (d) Immunofluorescence microscopy of albumin in liver. Liver sections from the mice were fixed and stained using rabbit antialbumin antibody and normal rabbit IgG as a negative control.

blotting, and found no apparent increase of P-PKR (data not shown). These results indicate that these target sequences and structures are of sufficient specificity to silence the target gene without eliciting non-specific interferon responses.

Beside the canonical action of siRNA, a sequence-specific cleavage of target mRNA, the siRNA could act as a micro-RNA

that suppresses translational initiation of mRNA,[38] or it could mediate transcriptional gene silencing.[39] Regarding our *in-vivo* experiments, it was difficult to differentially analyze the effect of siRNA at individual sites of action because post-translational effect of siRNA concomitantly destabilizes target mRNA, which leads to apparent decrease of mRNA transcripts.

Efficiency and safety of gene transfer methods are the key determinants of the clinical success of gene therapy and an unresolved problem. There are several reports of delivery of siRNA or siRNA-expression vectors to cells *in vivo*;[12,40,41] however, gene delivery methods that are safe enough to apply to clinical therapeutics are currently under development. Adenovirus vectors are one of the most commonly used carriers for human gene therapies.[42–44] Our present results demonstrate that the adenoviral delivery of shRNA is effective in blocking HCV replication *in vitro* and virus protein expression *in vivo*. Adenovirus vectors have several advantages of efficient delivery of transgene both *in vitro* and *in vivo* and natural hepatotropism when administered *in vivo*. The AxshRNA-HCV specifically blocked expression of HCV structural proteins in a conditional transgenic mouse expressing those proteins. The current adenovirus vectors may cause inflammatory reactions in the target organ,[45] however, and produce neutralizing antibodies which make repeated administration difficult. These problems may be overcome by the improved constructs of virus vectors with attenuated immunogenicity or by the development of non-viral carriers for gene delivery.[46]

In conclusion, our results demonstrate the effectiveness and feasibility of the siRNA expression system. The efficiency of adenovirus expressing shRNA that target HCV suggests that delivery and expression of siRNA in hepatocytes may eliminate the virus and that this RNA-targeting approach might provide a potentially effective future therapeutic option for HCV infection.

Acknowledgments

References

1 Alter MJ. Epidemiology of hepatitis C. *Hepatology* 1997; 26: 62S–65S.

2 Hadziyannis SJ, Sette H Jr, Morgan TR *et al.* Peginterferon-alpha2a and ribavirin combination therapy in chronic hepatitis C: a randomized study of treatment duration and ribavirin dose. *Ann. Intern. Med.* 2004; 140: 346–55.

3 Fire A, Xu S, Montgomery M, Kostas S, Driver S, Mello C. Potent and specific genetic interference by double-stranded RNA in Caenorhabditis elegans. *Nature* 1998; 19: 806–11.

4 Elbashir SM, Harborth J, Lendeckel W, Yalcin A, Weber K, Tuschl T. Duplexes of 21-nucleotide RNAs mediate RNA interference in cultured mammalian cells. *Nature* 2001; 411: 494–8.

5 Coburn GA, Cullen BR. Potent and specific inhibition of human immunodeficiency virus type 1 replication by RNA interference. *J. Virol.* 2002; 76: 9225–31.

6 Jacque JM, Triques K, Stevenson M. Modulation of HIV-1 replication by RNA interference. *Nature* 2002; 418: 435–8.

7 Gitlin L, Karelsky S, Andino R. Short interfering RNA confers intracellular antiviral immunity in human cells. *Nature* 2002; 418: 430–4.

8 Ge Q, Filip L, Bai A, Nguyen T, Eisen HN, Chen J. Inhibition of influenza virus production in virus-infected mice by RNA interference. *Proc. Natl. Acad. Sci. USA* 2004; 101: 8676–81.

9 Wang C, Pflugheber J, Sumpter R Jr *et al.* Alpha interferon induces

10 Klein C, Bock CT, Wedemeyer H *et al.* Inhibition of hepatitis B virus replication in vivo by nucleoside analogues and siRNA. *Gastroenterology* 2003; 125: 9–18.

11 Konishi M, Wu CH, Wu GY. Inhibition of HBV replication by siRNA in a stable HBV-producing cell line. *Hepatology* 2003; 38: 842–50.

12 McCaffrey AP, Meuse L, Pham TT, Conklin DS, Hannon GJ, Kay MA. RNA interference in adult mice. *Nature* 2002; 418: 38–9.

13 Shlomai A, Shaul Y. Inhibition of hepatitis B virus expression and replication by RNA interference. *Hepatology* 2003; 37: 764–70.

14 Yokota T, Sakamoto N, Enomoto N *et al.* Inhibition of intracellular hepatitis C virus replication by synthetic and vector-derived small interfering RNAs. *EMBO Rep.* 2003; 4: 602–8.

15 Kapadia SB, Brideau-Andersen A, Chisari FV. Interference of hepatitis C virus RNA replication by short interfering RNAs. *Proc. Natl. Acad. Sci. USA* 2003; 100: 2014–18.

16 Kronke J, Kittler R, Buchholz F *et al.* Alternative approaches for efficient inhibition of hepatitis C virus RNA replication by small interfering RNAs. *J. Virol.* 2004; 78: 3436–46.

17 Randall G, Grakoui A, Rice CM. Clearance of replicating hepatitis C virus replicon RNAs in cell culture by small interfering RNAs. *Proc. Natl. Acad. Sci. USA* 2003; 100: 235–40.

18 Seo MY, Abrignani S, Houghton M, Han JH. Letter to the editor: small interfering RNA-mediated inhibition of hepatitis C virus replication in the human hepatoma cell line Huh-7. *J. Virol.* 2003; 77: 810–12.

19 Wilson JA, Jayasena S, Khvorova A *et al.* RNA interference blocks gene expression and RNA synthesis from hepatitis C replicons propagated in human liver cells. *Proc. Natl. Acad. Sci. USA* 2003; 100: 2783–8.

20 Guo JT, Bichko VV, Seeger C. Effect of alpha interferon on the hepatitis C virus replicon. *J. Virol.* 2001; 75: 8516–23.

21 Tanabe Y, Sakamoto N, Enomoto N *et al.* Synergistic inhibition of intracellular hepatitis C virus replication by combination of ribavirin and interferon-alpha. *J. Infect. Dis.* 2004; 189: 1129–39.

22 Maekawa S, Enomoto N, Sakamoto N *et al.* Introduction of NS5A mutations enables subgenomic HCV-replicon derived from chimpanzee-infectious HC-J4 isolate to replicate efficiently in Huh-7 cells. *J. Viral. Hepat.* 2004; 11: 394–403.

23 Miyagishi M, Sumimoto H, Miyoshi H, Kawakami Y, Taira K. Optimization of an siRNA-expression system with an improved hairpin and its significant suppressive effects in mammalian cells. *J. Gene Med.* 2004; 6: 715–23.

24 Li Y, Yokota T, Matsumura R, Taira K, Mizusawa H. Sequence-dependent and independent inhibition specific for mutant ataxin-3 by small interfering RNA. *Ann. Neurol.* 2004; 56: 124–9.

25 Kanazawa N, Kurosaki M, Sakamoto N *et al.* Regulation of hepatitis C virus replication by interferon regulatory factor-1. *J. Virol.* 2004; 78: 9713–20.

26 Wakita T, Pietschmann T, Kato T *et al.* Production of infectious hepatitis C virus in tissue culture from a cloned viral genome. *Nat. Med.* 2005; 11: 791–6.

27 Zhong J, Gastaminza P, Cheng G *et al.* Robust hepatitis C virus infection in vitro. *Proc. Natl. Acad. Sci. USA* 2005; 102: 9294–9.

28 Wakita T, Taya C, Katsume A *et al.* Efficient conditional transgene expression in hepatitis C virus cDNA transgenic mice mediated by the Cre/loxP system. *J. Biol. Chem.* 1998; 273: 9001–6.

29 Kashiwakuma T, Hasegawa A, Kajita T *et al.* Detection of hepatitis C virus specific core protein in serum of patients by a sensitive fluorescence enzyme immunoassay (FEIA). *J. Immunol. Methods* 1996; 28: 79–89.

30 Baglioni C, Nilsen TW. Mechanisms of antiviral action of interferon. *Interferon* 1983; **5**: 23–42.

31 Bridge A, Pebernard S, Ducraux A, Nicoulaz A, Iggo R. Induction of an interferon response by RNAi vectors in mammalian cells. *Nat. Genet.* 2003; **34**: 263–4.

32 Carmichael GG. Silencing viruses with RNA. *Nature* 2002; **418**: 379–80.

33 Okamoto H, Okada S, Sugiyama Y *et al.* Nucleotide sequence of the genomic RNA of hepatitis C virus isolated from a human carrier: comparison with reported isolates for conserved and divergent regions. *J. Gen. Virol.* 1991; **72**: 2697–704.

34 Kato T, Date T, Miyamoto M *et al.* Efficient replication of the genotype 2a hepatitis C virus subgenomic replicon. *Gastroenterology* 2003; **125**: 1808–17.

35 Alexopoulou L, Holt AC, Medzhitov R, Flavell RA. Recognition of double-stranded RNA and activation of NF-kB by Toll-like receptor 3. *Nature* 2001; **413**: 732–8.

36 Yoneyama M, Kikuchi M, Natsukawa T *et al.* The RNA helicase RIG-I has an essential function in double-stranded RNA-induced innate antiviral responses. *Nat. Immunol.* 2004; **5**: 730–7.

37 Sledz C, Holko M, de Veer M, Silverman R, Williams, B. Activation of the interferon system by short-interfering RNAs. *Nat. Cell. Biol.* 2003; **5**: 834–9.

38 Doench JG, Petersen CP, Sharp PA. siRNAs can function as miRNAs. *Genes Dev.* 2003; **17**: 438–42.

39 Morris KV. siRNA-mediated transcriptional gene silencing: the potential mechanism and a possible role in the histone code. *Cell. Mol. Life Sci.* 2005; **62**: 3057–66.

40 Xia H, Mao Q, Paulson HL, Davidson BL. siRNA-mediated gene silencing in vitro and in vivo. *Nat. Biotechnol.* 2002; **20**: 1006–10.

41 Zender L, Hutker S, Liedtke C *et al.* Caspase 8 small interfering RNA prevents acute liver failure in mice. *Proc. Natl. Acad. Sci. USA* 2003; **100**: 7797–802.

42 Akli S, Caillaud C, Vigne E *et al.* Transfer of a foreign gene into the brain using adenovirus vectors. *Nat. Genet.* 1993; **3**: 224–8.

43 Bajocchi G, Feldman SH, Crystal RG, Mastrangeli A. Direct in vivo gene transfer to ependymal cells in the central nervous system using recombinant adenovirus vectors. *Nat. Genet.* 1993; **3**: 229–34.

44 Davidson BL, Allen ED, Kozarsky KF, Wilson JM, Roessler BJ. A model system for in vivo gene transfer into the central nervous system using an adenoviral vector. *Nat. Genet.* 1993; **3**: 219–23.

45 Yang Y, Wilson JM. Clearance of adenovirus-infected hepatocytes by MHC class I-restricted CD4+ CTLs in vivo. *J. Immunol.* 1995; **155**: 2564–70.

46 Fleury S, Driscoll R, Simeoni E *et al.* Helper-dependent adenovirus vectors devoid of all viral genes cause less myocardial inflammation compared with first-generation adenovirus vectors. *Basic Res. Cardiol.* 2004; **99**: 247–56.

ALS-linked mutant SOD1 induces ER stress- and ASK1-dependent motor neuron death by targeting Derlin-1

Hideki Nishitoh, Hisae Kadowaki, Atsushi Nagai, et al.

Supplemental Material	http://genesdev.cshlp.org/content/suppl/2008/06/03/22.11.1451.DC1.html
References	This article cites 50 articles, 24 of which can be accessed free at: **http://genesdev.cshlp.org/content/22/11/1451.full.html#ref-list-1**
	Article cited in: **http://genesdev.cshlp.org/content/22/11/1451.full.html#related-urls**
Email alerting service	Receive free email alerts when new articles cite this article - sign up in the box at the top right corner of the article or **click here**

To subscribe to *Genes & Development* go to:
http://genesdev.cshlp.org/subscriptions